JAERI-M
9246

FATIGUE TEST RESULTS OF STRAIGHT PIPE WITH FLAWS IN INNER SURFACE

January 1981

Katsuyuki SHIBATA, Toshihiro OBA, Takaichi KAWAMURA
Norio YOKOYAMA* and Shohachiro MIYAZONO

日本原子力研究所
Japan Atomic Energy Research Institute

JAERI-M 9246

Fatigue Test Results of Straight Pipe with Flaws in Inner Surface

Katsuyuki SHIBATA, Toshihiro OBA, Takaichi KAWAMURA
Norio YOKOYAMA* and Shohachiro MIYAZONO

Division of Reactor Safety, Tokai Research Establishment, JAERI

(Received November 29, 1980)

Fatigue and fracture tests of piping models with flaws in the inner surface were carried out to investigate the fatigue crack growgh, coalescence of multiple cracks and fracture behavior.

Two straight test pipes with and without weldment in the test section of SUS304L stainless steel were tested under almost the same test conditions. Three artificial defects were machined in the inner surface of the test section of the test pipes.

The fatigue test were performed untill the cracks coalesced and grew through the thickness. Subsequently, a static load was imposed on test pipe which contained a large crack in the test section.

The test results show that the fatigue crack growth is slower than that predicted by the method specified in the SectionXI of ASME Boiler and Pressure Vessel Code, and that the test pipes can endure more than the static load of 3Sm without an unstable fracture.

Keywords : Fatigue, Crack Growth, Coalescence, Straight Pipe, Fracture, SUS304L Stainless Steel

---

This work was performed under the contract between the Science and Technology Agency of Japan and JAERI to demonstrate the integrity for fatigue life of the primary coolant pipes in nuclear power plants.

* On leave from Kurs Science and Engineering Co. Ltd.

JAERI－M 9246

複数の内面欠陥を有する直管試験体の疲労試験結果

日本原子力研究所東海研究所安全工学部
柴田　勝之・大場　敏弘・川村　隆一
横山　憲夫*・宮園　昭八郎

（１９８０年１１月２９日受理）

外径約３００mm のＳＵＳ３０４Ｌステンレス鋼管を供試管に使用し，内面に複数の欠陥を有する直管試験体の疲労および破壊試験を実施した。試験は溶接継手付試験体および母材試験体の２つのケースについて行い，試験体内面に加工した３個の人工欠陥からのき裂発生，伝播，合体等の挙動を調べた。き裂が大きな内面欠陥へと成長し，わずかに肉厚を貫通した時点で疲労試験を終了し，その後，大きな内面欠陥付の試験体に静的に荷重を負荷することにより破壊試験を実施し，破壊の進行についても調べた。

疲労き裂の伝播計測には超音波探傷法，スメックゲージ法，およびビーチマーク法を用い良好な測定結果を得た。また破壊試験では写真撮影によって試験体外表面におけるき裂進展を測定した。

今回実施した疲労試験に関してＡＳＭＥ Code に定められた方法により，き裂伝播挙動を解析し実験結果と比較した。その結果ＡＳＭＥ Code の方法は安全側の予測となることが分った。さらに破壊試験の結果から試験体内面に大きな欠陥がある場合でも，ＡＳＭＥ Code で規定される３Sm の静荷重に試験体は耐え得ることが分った。

この報告書は，電源開発促進対策特別会計施行令に基き，科学技術庁から日本原子力研究所への委託研究，昭和５３年度配管信頼性実証試験のうち直管試験体の配管疲労試験結果についてまとめたものである。

＊　外来研究員；クールス科学技術（株）

Contents

Nomenclature

1. Introduction 1

2. Test pipes 3

2.1 Chemical compositions and mechanical properties of test pipe 3

2.2 Fabrication of the test pipes 3

3. Tests 6

3.1 Loading conditions 6

3.2 Test procedure 7

3.3 Strain and displacement measurement 8

3.4 Crack extension measurement 8

4. Strain measurement results 15

5. Fatigue test results 19

5.1 Fatigue crack growth measurements 19

5.2 Crack Growth rate 21

5.3 Comparison of crack growth 21

6. Fracture test results 34

6.1 Results of strain and displacement measurement 34

6.2 Results of crack extension measurement 34

6.3 Summary of fracture test 35

7. Fractographic observation 50

8. Conclusions 51

Acknowledgement 52

Reference 52

目　　次

記号表
1. まえがき …… 1
2. 試験体 …… 3
2.1 供試管の化学成分および機械的性質 …… 3
2.2 試験体の製作 …… 3
3. 試験方法 …… 6
3.1 荷重条件 …… 6
3.2 試験手順 …… 7
3.3 歪および変位測定方法 …… 8
3.4 き裂伝播測定方法 …… 8
4. 歪測定結果 …… 15
5. 疲労試験結果 …… 19
5.1 疲労き裂伝播測定結果 …… 19
5.2 き裂伝播速度 …… 21
5.3 実験結果とき裂伝播解析結果の比較 …… 21
6. 破壊試験結果 …… 34
6.1 歪測定および変位測定結果 …… 34
6.2 き裂進展測定結果 …… 34
6.3 破壊試験結果のまとめ …… 35
7. フラクトグラフィーによる破面観察 …… 50
8. 結　論 …… 51
謝　辞 …… 52
参考文献 …… 52

Nomenclature

a,	half crack length of through thickness crack or minor half diameter of elliptical (semi-elliptical) crack
b,	major half diameter of elliptical (semi-elliptical) crack
k,	stress intensity factor
Δk,	range of stress intensity factor
$\Delta\sigma$,	range of applied stress
σ_{max},	maximum of applied stress
σ_{min},	minimum of applied stress
R,	stress ratio
N,	number of cycles
σ_θ,	circumferential stress
σ_L,	longitudinal stress
ε_θ,	circumferential strain
ε_L,	longitudinal strain
t,	wall thickness
D_o,	outer diameter
D_i,	inner diameter
r,	radius
E,	modulus of elasticity
σ_{YS},	0.2% yield strength
ν,	Poisson's ratio
I,	plane moment of inertia
P,	applied load
p,	range of
ΔP,	range of applied load
δ,	displacement
Pm,	general primary manbrance stress intensity
Pb,	primary bending stress intensity
P_L,	local manbrance stress intensity
S_m,	design stress intensity value
S_y,	specified minimum yield strength
B_1, B_2,	primary stress indices
Q,	flaw shape parameter
M_m,	manbrane stress correction factor
M_b,	bending stress correction factor

1. Introduction

The structural components of light-water-cooled nuclear power reactors are installed based on lots of experience which various conventional power plants have had for a long period. The piping system, one of the structural components, is attentively designed, fabricated, installed and inspected so that the integrity and safety of nuclear power reactors are assured in the normal operating conditions and postulated accident conditions. In spite of considering the piping safety and performance in the design and construction of structural component, based on various standards, criteria and so on, many piping failures have been reported in nuclear power plants to date. However, sudden flaw-induced piping fractures have not been caused, i.e. the piping failures detected are the part-through cracks without leakage or the through cracks with small leakage. On the other hand, in the piping system of light-water-cooled nuclear power reactors a instantaneous guillotine or slot rupture is assumed as one of the design base accidents and protection against the damages of adjacent structural components resulting from an excessive loss of coolant is provided by employing the protective systems. The guillotine or slot rupture of the pipe assumes that the pipe breaks instantaneously in the circumferential or axial direction and the high temperature fluid flows from the opening areas of the pipe.

As previously mentioned, the sudden ruptures of the pipe have not been caused to date and also in the future such failures of the pipe in nuclear power reactors are considered to be extremely unlikely. However, one of the desirable safety features of the piping system is to predict a serious situation before it develops. It is very important to the piping safety and performance to understand how defects might propagate from initial flaws, grow through the wall of piping components and how they might sever. If the severance of the piping components in nuclear power reactors might occur, it might develop through the following assumptions;

1) Initial flaws are caused in the inner surface or sub-surface of piping components during their fabrication by cyclic loads imposed during transients or stress corrosion.
2) The initial flaws grow to very long part-through cracks by fatigue, stress corrosion and so on.

3) The long part-through cracks are severed by the extraordinary loads (such as earthquake or water hammer) imposed during the operation of nuclear power reactors.

The fatigue and fracture tests of piping models reported herein have been carried out to investigate the above processes using two straight pipe models, 320 mm in outer diameter, of SUS 304 L stainless steel under almost the same test conditions. Three artificial defects were provided in the inner surface of the test pipes along the circumferential direction by a Electrical Discharge Machining (EDM). Those artificial defects were machined in the base metal of one test pipe and in the heat affected zone of welds of another test pipe.

Firstly, cyclic bending moments were imposed to investigate the fatigue crack growth behavior and coalescence of those cracks and secondly, after those grew through the wall of the test section, a static bending moment was imposed to investigate the fracture behavior, such as strain or stress distribution, deformation and crack extension of the test pipes.

2. Test pipes

2.1 Chemical compositions and mechanical properties of test pipe

SUS 304 L stainless steel pipe was used in the tests. It is an improved type stainless steel of low carbon and high nitrogen content against stress corrosion cracking in high temperature water environment, and has an equivalenet mechanical properties to conventional material.

The test pipes used are the stainless steel pipes of 320 mm in outer diameter and 35 mm in thickness and have the chemical compositions and mechanical properties as shown in Table 2.1.

2.2 Fabrication of test pipes

A cantilever type test pipe fixed on the test bed was used considering the feasibility of measurements and loading system. The hydraulic actuater of 63 ton capacity was fixed on the reaction wall. The test pipe geometry is shown in Fig.2.1.

Tests were performed on two straight test pipes, ST-1 and ST-2. In one test pipe (ST-2) was provided a butt weld in the test section, and in another was used a base metal in the test section. The weldment of the ST-2 test pipe is shown in Fig.2.1 in detail, and weld procedure and conditions are shown in Table 2.2.

In the test of ST-2 test pipe, three artificial defects were machined by EDM in the heat affected zone; 15 mm from the center of weld beads, and 500 mm from the bottom of the test pipe. The artificial defects of the ST-1 test pipe were machined in the same location with the ST-2 test pipe.

Table 2.1 Chemical compositions and mechanical properties of the test pipes

		C	Si	Mn	P	S	Ni	Cr	N
Spec.	Min.	——	——	——	——	——	8.00	18.00	——
	Max.	0.02	1.00	2.00	0.040	0.030	11.00	20.00	0.12
0922305	Ladle	0.011	0.52	1.68	0.024	0.001	10.35	18.35	0.941
(5 - 8)	Check	0.012	0.52	1.68	0.024	0.001	10.45	18.35	0.957

		0.2 YS. kg/mm^2	U TS kg/mm^2	Elong. %	Hardness HB	Grain Size No.
Spec.	Min.	21	53	35	——	——
	Max.	——	——	——	——	——
0922305 (5 - 8)	L-	28	59	64	153 151	5.2
	Direc.	27	58	64	150 151	

(1) Tensile Specimen: JIS No.4 GL = 50mm D = 14mmϕ

(2) Heat Treatment : 1060°C × 30MIN WQ.

Table 2.2 Welding procedure of test pipes

method	GTAW(first layer) + SMAW
shape of edge prep.	U type
welding rod	GTAW: TGS-308LK, 3.2~4ϕ SMAW: NC-38LK, 1.6~2ϕ
pre-heat	no
stress relief	no
shield gas	argon gas
back surface protection	argon gas
welding current and voltage	GTAW: 60~145A, 15V SMAW: 60~145A, 30V
welding position	flat
No. of layers	GTAW: 1, SMAW: 7
finish	as weld

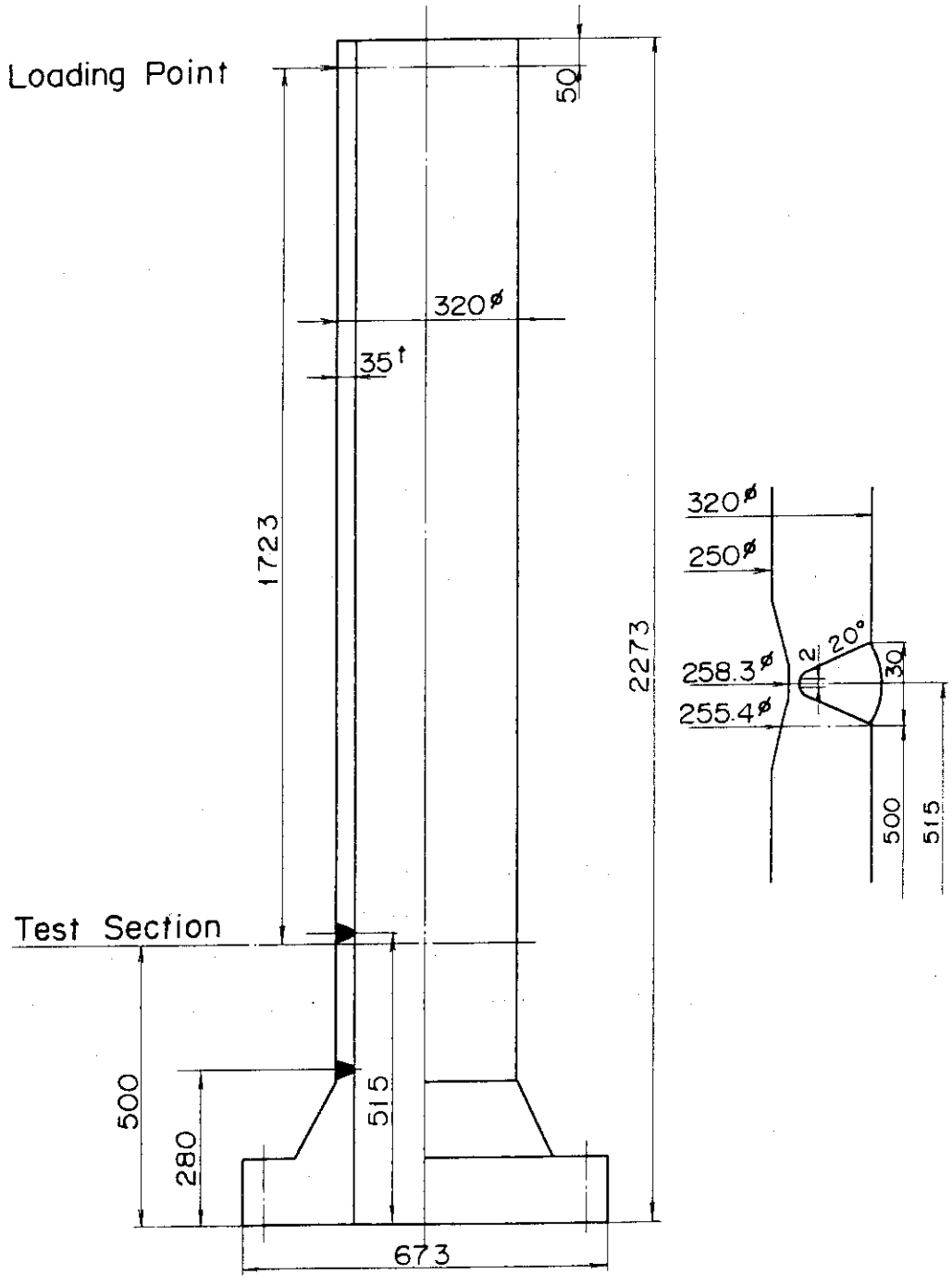

Fig.2.1 Geometry of the test pipe (mm)

3. Tests

3.1 Loading conditions

The limits of stress intensities in the structural components of nuclear power reactor are described in the Section III of ASME Boiler and Pressure Vessel Code[1]. In the design condition primary stress intensities are specified as follows:

$$P_m \leqq S_m$$
$$P_L \leqq 1.5\ S_m$$
$$P_L + P_b \leqq 1.5\ S_m$$

In the straight pipe subject to moment load, the stress intensity limit is as follows:

$$P_b = B_2 \frac{D_o}{2I} \leqq 1.5\ S_m$$

$$B_2 = 1.0$$

As an allowable stress is generally determined on the base of S_m value, the S_m or 1.5 S_m value was taken as a reasonable stress range of the fatigue test. However, since it was difficult to carry out the fatigue test under 1.5 S_m value due to limitation of the test apparatus and test pipe, the fatigue stress conditions were determined as follows:

$$\Delta\sigma = S_m$$

$$R = \sigma_{min} / \sigma_{max} = 0.1$$

The S_m and S_y values of the test pipe defined are as follows:

$$S_m = 14.0\ kg/mm^2$$

$$S_y = 21.0\ kg/mm^2$$

The loads equivalent to S_m, S_y, CL (collapse load) and 3 S_m in the ST-1 and ST-2 test pipes are the following values:

P = 15.6 ton ---------- S_m
= 23.4 ton ---------- S_y or 1.5 S_m
= 35.1 ton ---------- CL or 1.5 S_y
= 46.8 ton ---------- 3 S_m

The section factor, K is defined in the Section III, Appendix A.

$$K = \frac{32}{6\pi} \frac{1-(D_i/D_o)^3}{1-(D_i/D_o)^4} = 1.41$$

Therefore, in the cylindrical cross section of the test pipe, the collapse load is obtained as follows:

P = 33.0 ton ---------- 1.41 S_y

The fatigue tests were carried out at the cyclic rate of 5 Hz considering the capacity of the apparatus and the test period. The geometry and position of artificial defects were decided considering the following conditions:

1) The fatigue test would be completed within $0.5 * 10^6$ to $1.0 * 10^6$ cycles under the stress range of S_m
2) The cracks would coalesce mutually and grow to a large single part-through crack before the penetration.

From the above viewpoints, three semi-elliptical defects of 8 mm in depth and 24 mm in length were machined in the inner surface of the test pipes in the same circumfrential cross section. Each crack interval was decided to be 1.75 t at the circumferential line of half thickness. The fatigue test conditions of ST-1 and ST-2 test pipes are summarized in Table 3.1.

3.2 Test procedures

The fatigue test was stopped when the crack penetrated to the outer surface. Subsequently an overload was imposed on the test pipe at the constant rate of 0.5 mm/sec so that it was deformed to the end displacement of 200 mm under displacement control mode. During the fracture test, strain and crack extension were measured by strain gages and electric potential method, holding the actuater position

temporarily.

The fatigue test apparatus of piping models was used in the test. The test system is schematized in Fig.3.1.

3.3 Strain and displacement measurement

Sixty uni-axial and rosette type strain gages were bonded on the test pipe to measure the stress distribution and four displacement gages were mounted. The location of strain and displacement gages is shown in Figs.3.2 and 3.3.

The strain and displacement were measured at the fatigue cycles of N = 1, 10, 100, and so on by a digital strain instrument. The test apparatus was held stepwise under constant load during the measurement.

In the fracture test, the output of displacement and load was connected to a X-Y recorder to obtain the relationship between load and displacement.

3.4 Crack extension measurement

In the fatigue test, some methods described below were applied to the crack size measurement.

1) Crack depth measurement by ultrasonic flow dedection

It is known that a high peak echo is reflected from a crack tip in the ultrasonic flaw detection. Crack depth can be calculated if the location of crack tip is detected. The principle of the peak echo technique is shown in Fig.3.4. The 5 MHz angle probe of longiludinal wave was used in the measurement.

2) Electric potential measurement

Electric potential measurement was performed to detect the crack extension, and its probes were attached at the following five locations; the center of each crack (3 locations) and center between two cracks (2 locations). The latter two probes were used to detect the coalescence of two cracks.

The electric potential measurement is shown in Fig.3.5.

3) Application of a crack front marking technique

A crack front marking technique (so called beach mark) was applied to leave crack front marks in the fracture surface by

changing the fatigue stress range and stress ratio as shown in Fig.3.6. The load, as shown in Fig.3.6, was applied at each time when the crack extension was about 2.5 mm in depth.

Besides the above crack growth measurement, the crack extension of the circumferential direction in the inner surface of the test pipe was observed by a video camera and monitor during the fatigue test.

After the fatigue test, the fracture test was carried out by imposing an overload. In this test, the length and the crack opening displacement of the through thickness crack were measured in the circumferential direction of the outer surface of the test pipe.

The digitally displayed load and displacement of the hydraulic actuator were measured by two synchronized photographic cameras at 0.5 or 0.25 flame per second (FPS). This measuring system is shown in Fig.3.7.

The electric potential measurement also was used in the fracture test using the same probes as the fatigue test.

Table 3.1 Fatigue test conditions

loading conditions	load : P = 1.73 ⇄ 17.3 ton stress* : σ_L = 1.6 ⇄ 15.6 Kg/mm^2 $\Delta\sigma$ = 14.0 Kg/mm^2 (= S m) stress ratio : R = 0.1 cyclic rate : f = 5 Hz
shape of artificial defects (unit = mm)	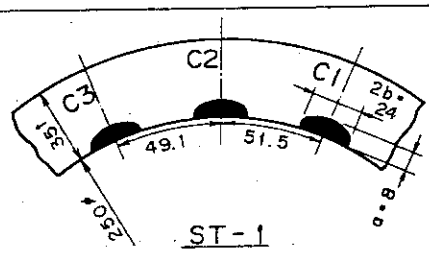 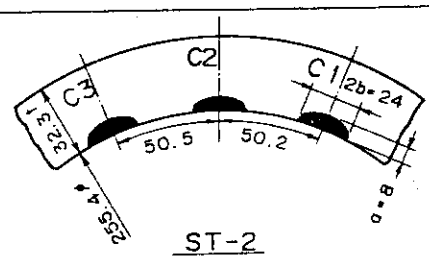

* Do = 318mm and t = 33.3 mm (JIS) were used

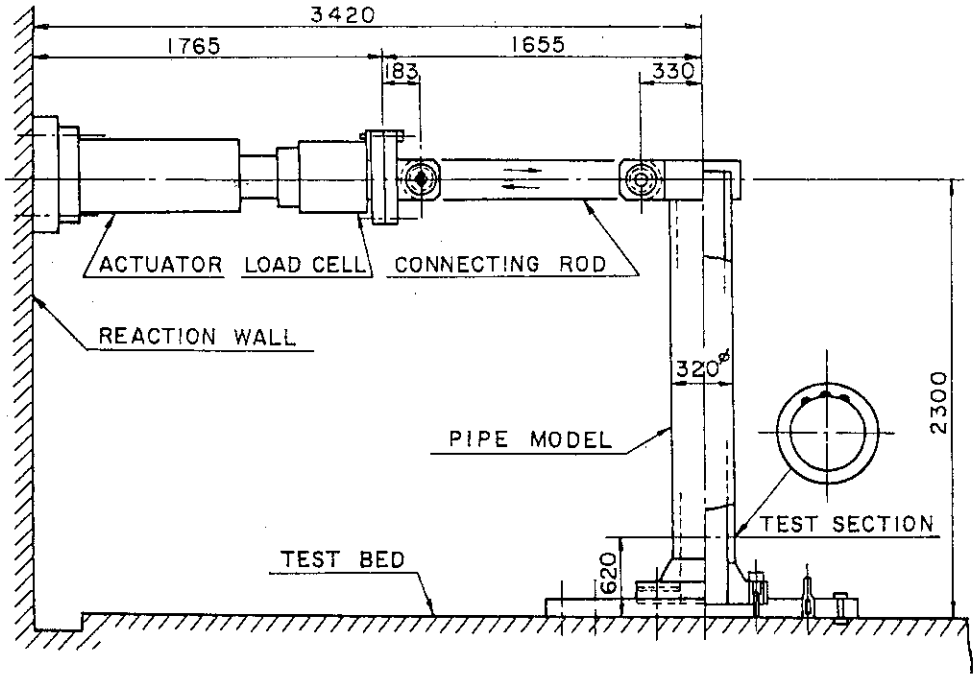

Fig. 3.1 Schematic view of the test system

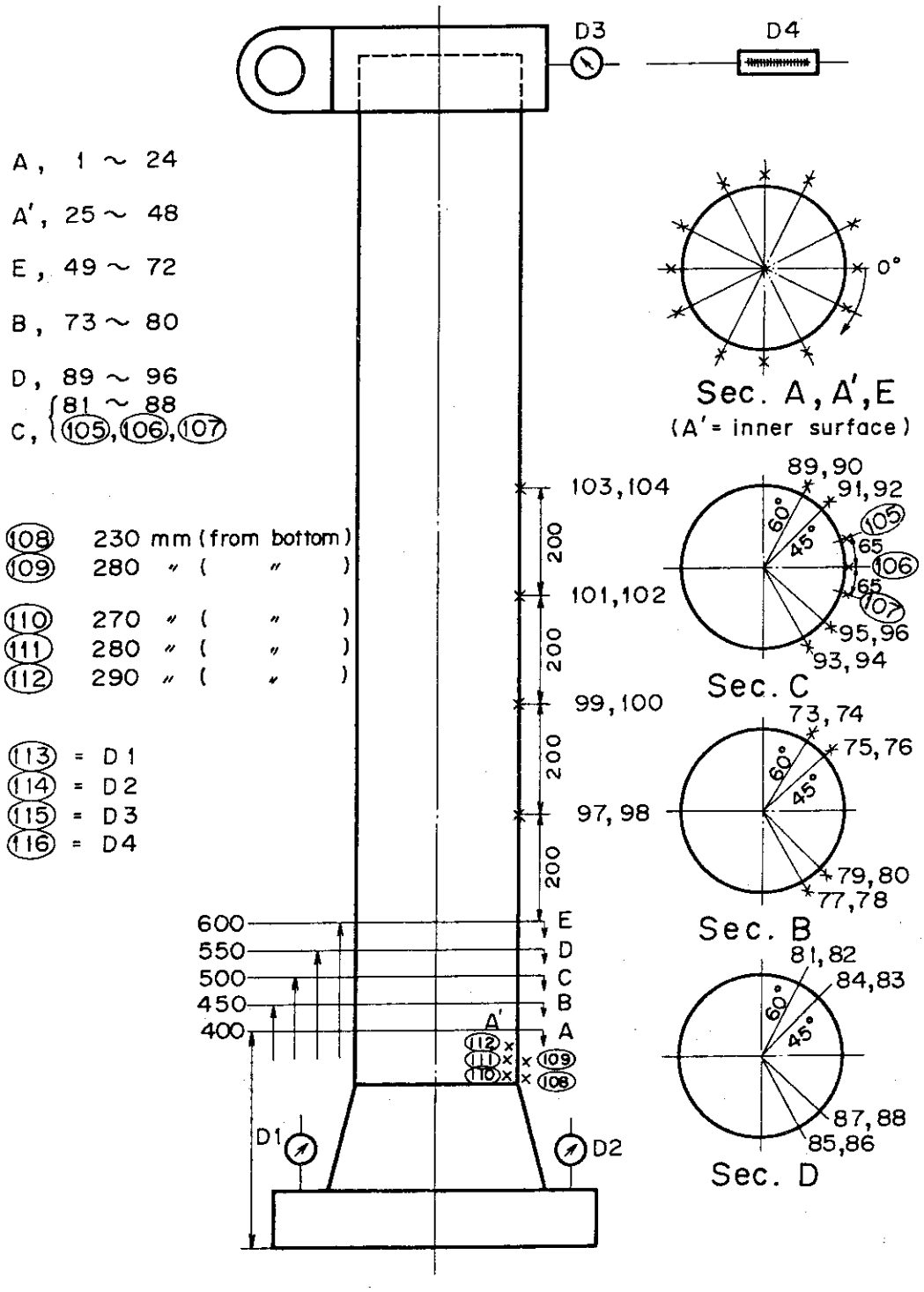

Fig. 3.2 Location of strain gages and displacement gages (ST - 1)

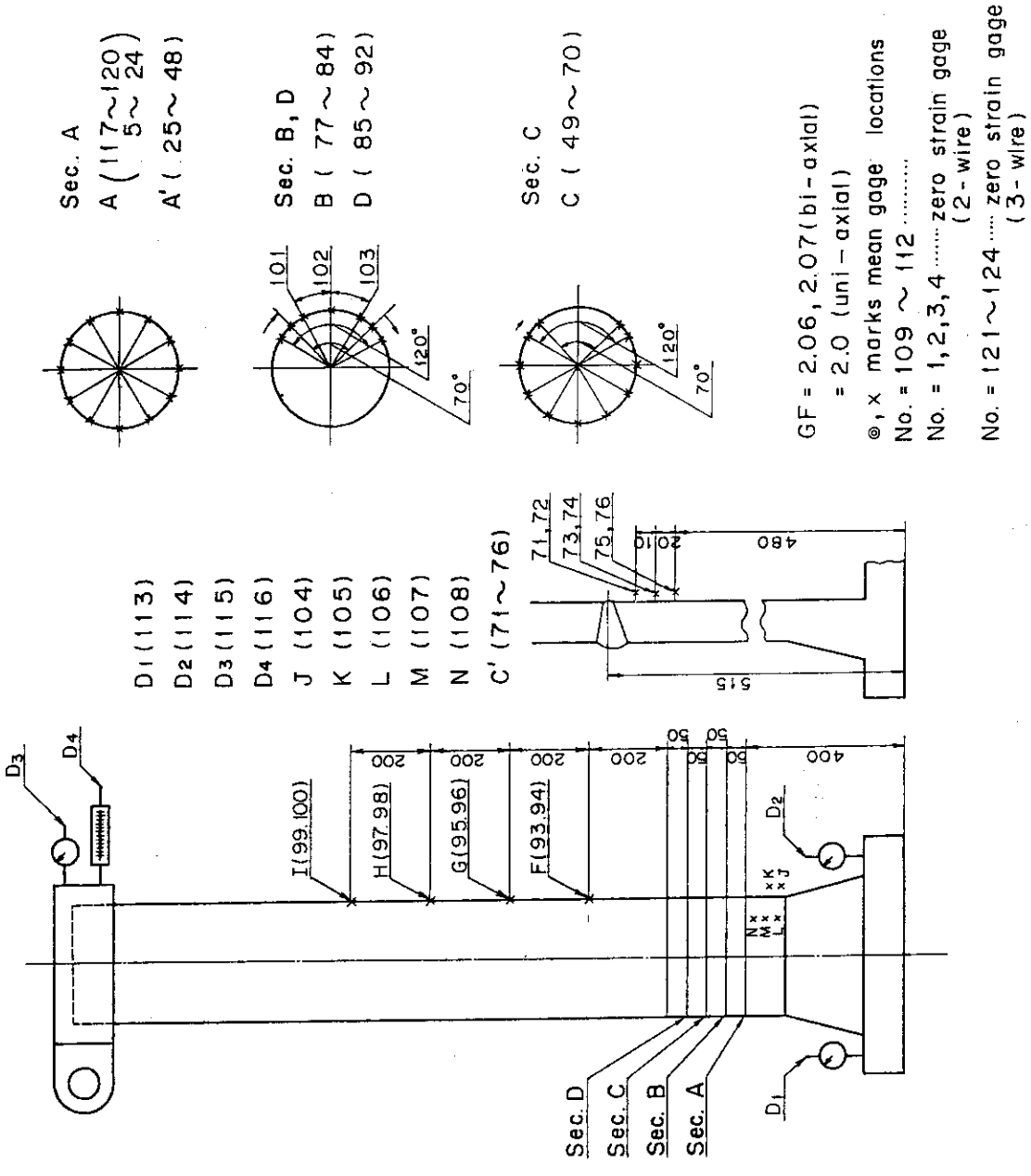

Fig. 3.3 Location of strain gages and displacement gages (ST-2)

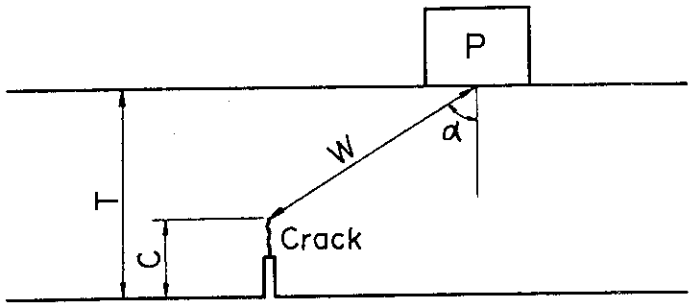

$C = T - W\cos\alpha$

P : Probe
T : Thickness
W : Beam Path
α : Reflaction angle
C : Crack Depth

Fig. 3.4 Principle of crack depth measurement by UT examination

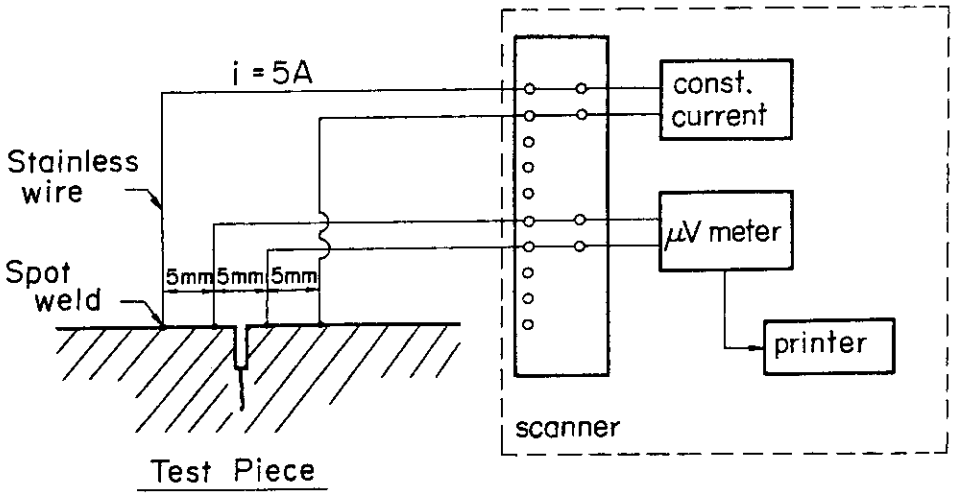

Fig. 3.5 Electric potential measurement

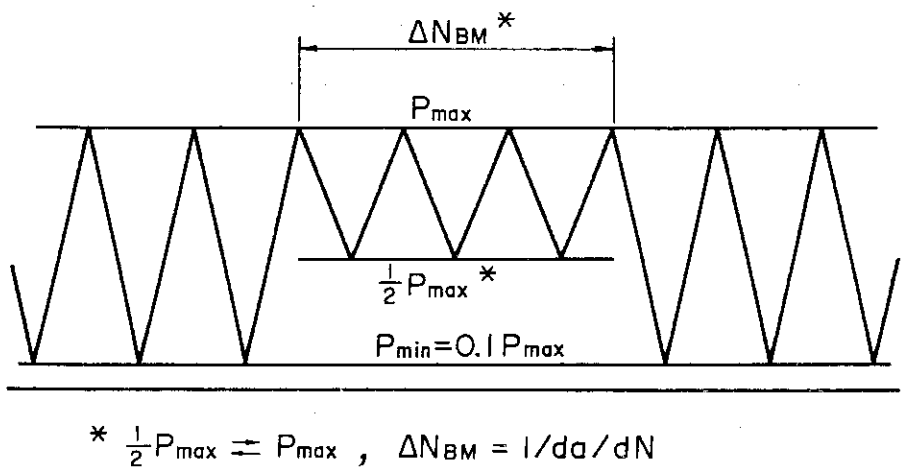

Fig. 3.6 Loading sequence of crack front marking

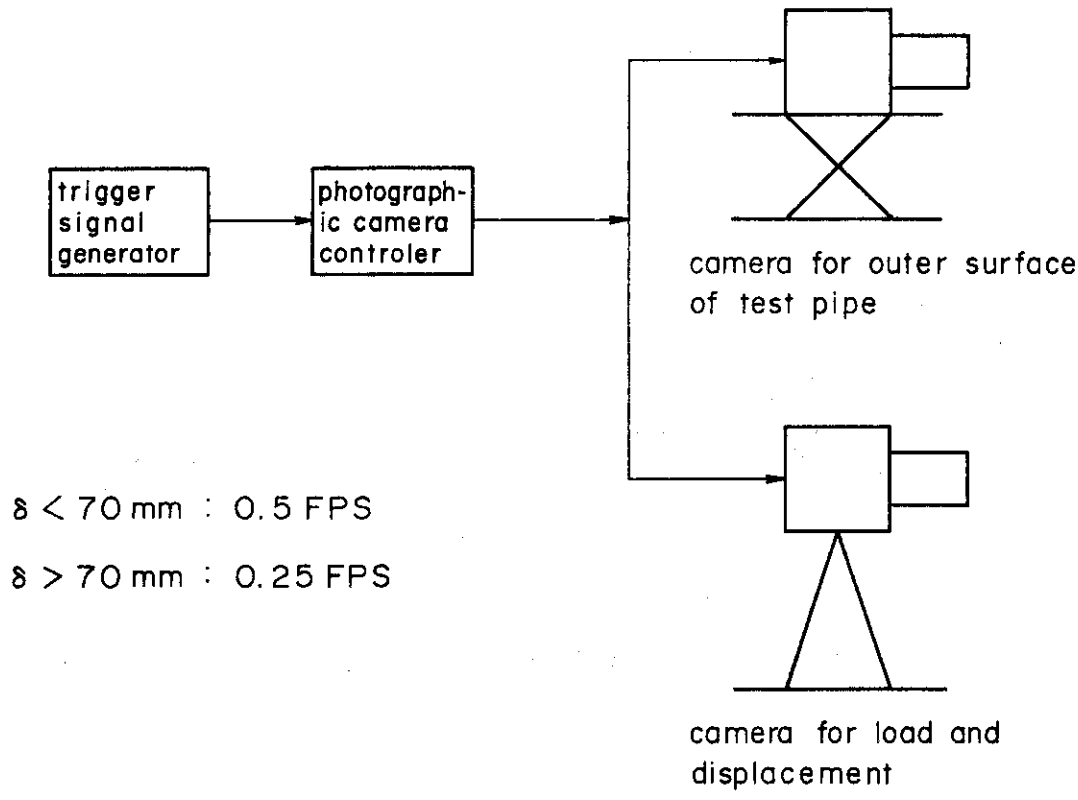

Fig. 3.7 Photographic camera system of crack extension measurement

4. Strain measurement results

The strain and displacements were measured at the fatigue cycles of N = 1, 10, 100, and so on by a digital strain instrument.

The results of the strain measurement at the first cycle are shown by the stress distributions of inner and outer surface of the test pipes.

Stresses were calculated using the following relationship:

$$\sigma_\theta = \frac{\varepsilon_\theta + \nu\ \varepsilon_L}{1-\nu^2} E$$

$$\sigma_L = \frac{\varepsilon_L + \nu\ \varepsilon_\theta}{1-\nu^2} E$$

The longitudinal stress distributions obtained by the test were compared with the calculated those based on the beam theory.

$$\sigma_L = \frac{M}{I} r \cos\theta$$

As typical examples, the experimental and calculated stress distributions of the Sec.A, A′, and E of ST-1 test pipe are compared in Figs.4.1 to 4.3 and those of the Sec.A, A′, and C of ST-2 test pipe in Figs.4.4 to 4.6.

As shown in Figs.4.1 to 4.3, the both stress distributions show good agreement, and as shown in Figs.4.4 to 4.6, the stress distributions of ST-2 test pipe are almost the same as those of ST-1.

It is estimated from Figs.4.1 to 4.3 that the stress status is almost uni-axial, since the longitudinal stress is considerably larger than the circumferential stress.

Almost the same stress distributions are seen too in Figs.4.4 to 4.6, in the case of ST-2 test pipe.

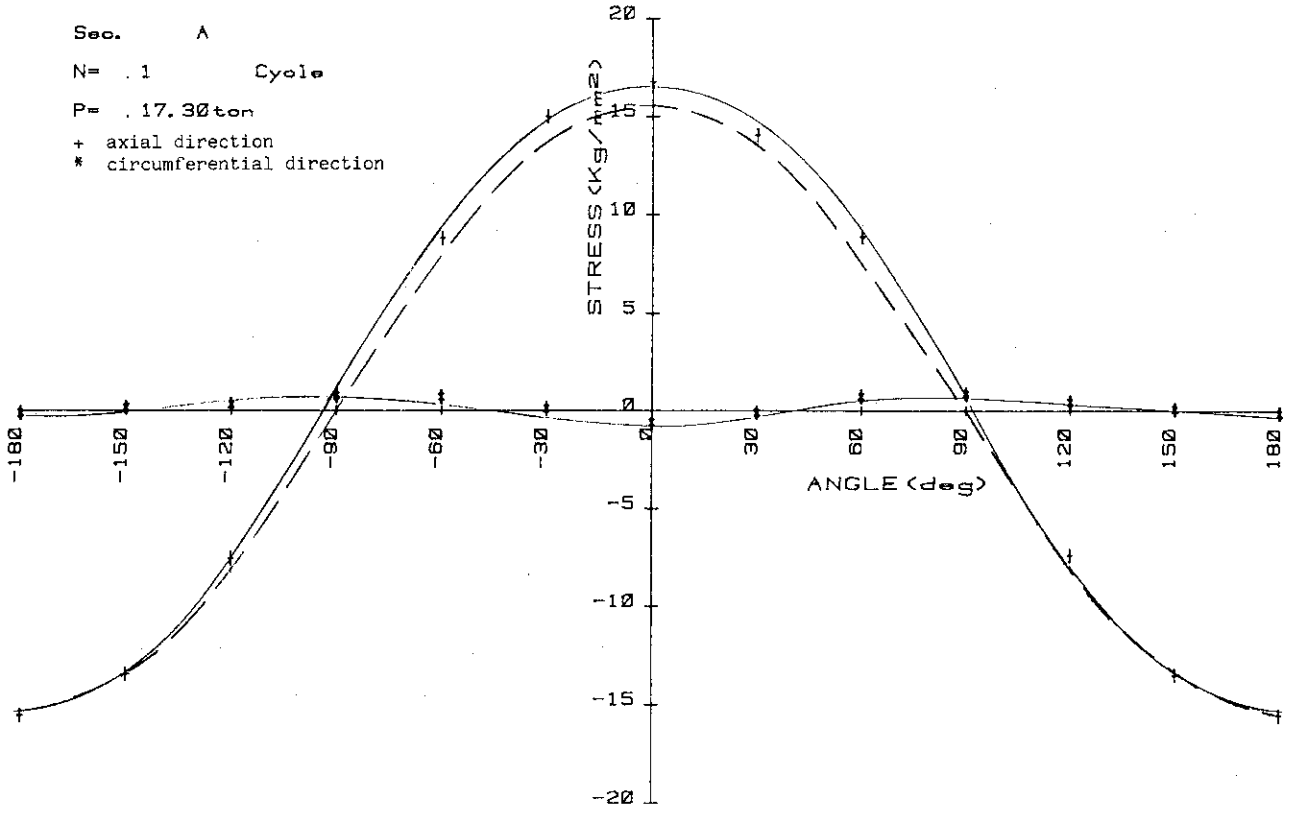

Fig. 4.1 Stress distribution (ST-1)

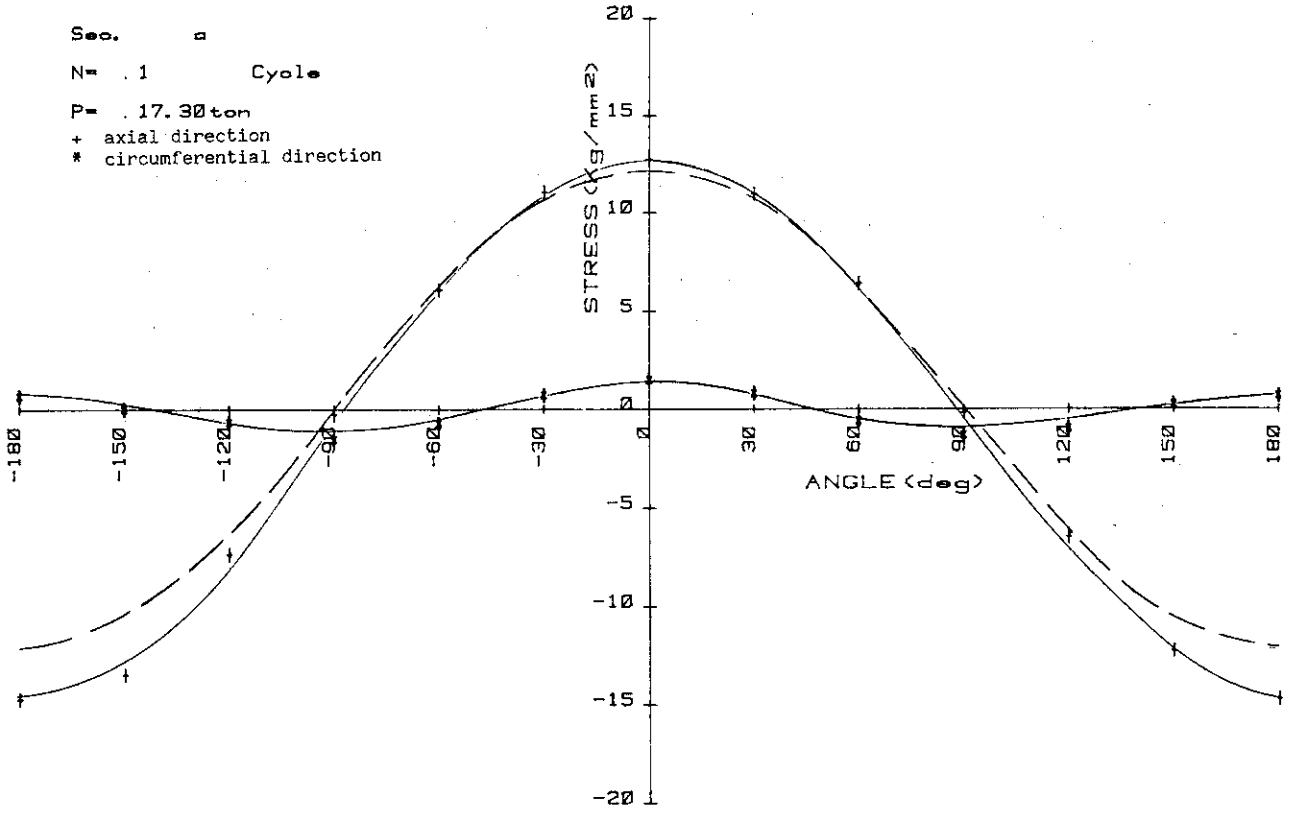

Fig. 4.2 Stress distribution (ST-1)

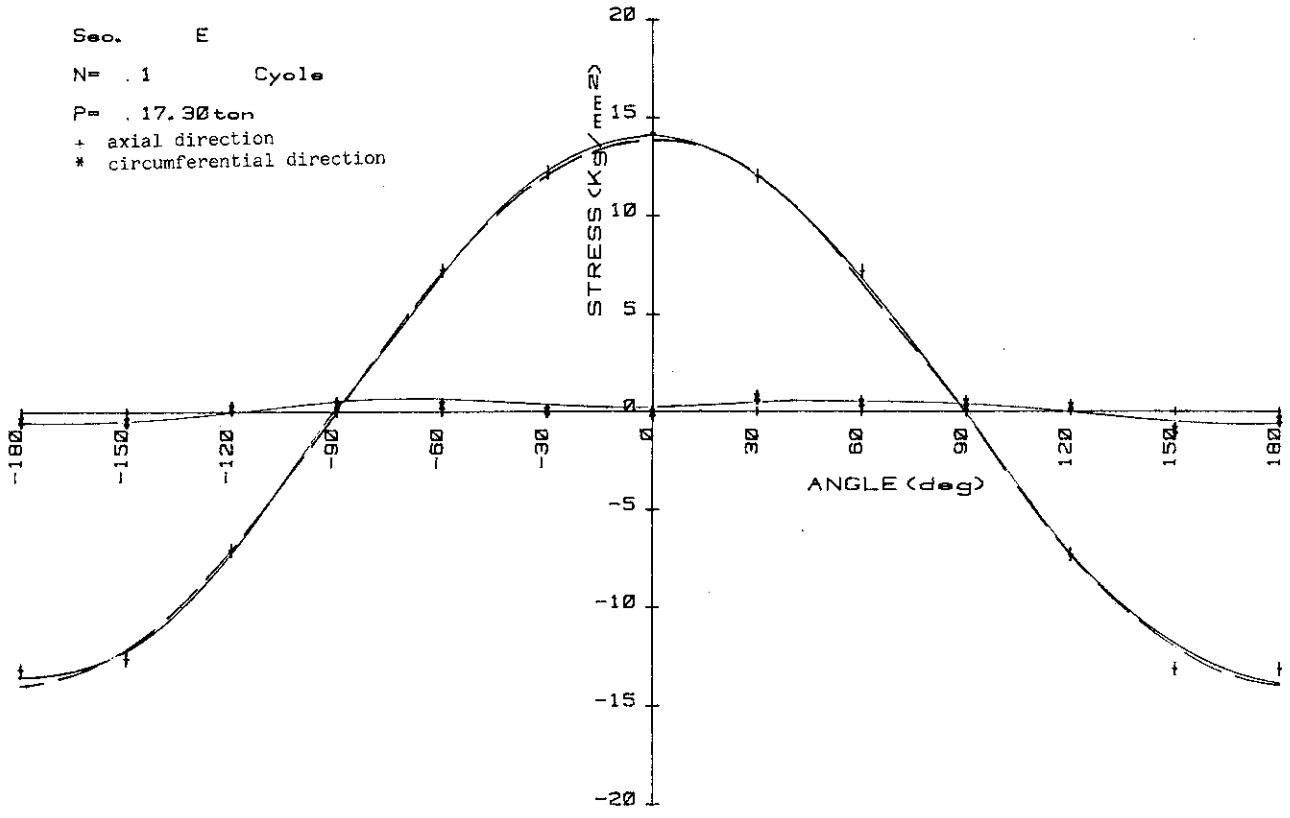

Fig. 4.3 Stress distribution (ST-1)

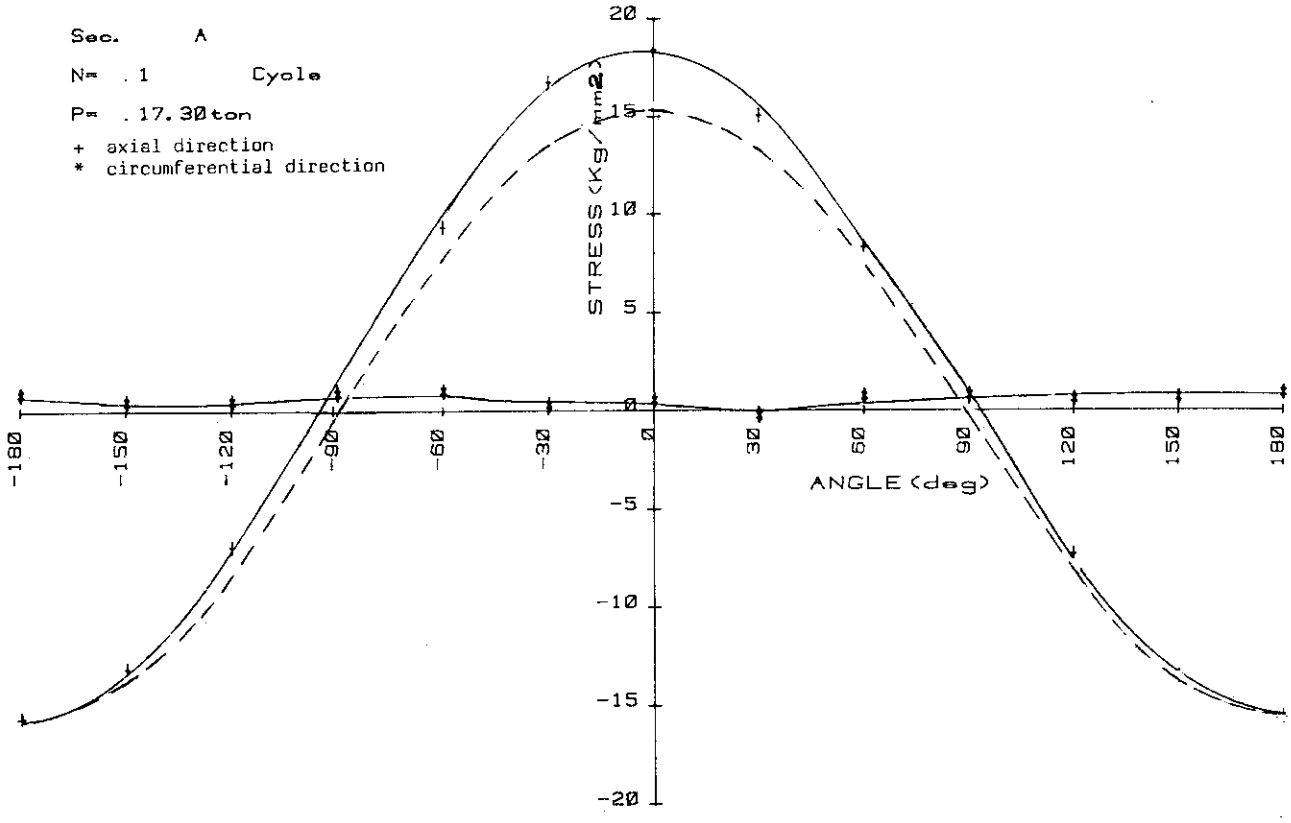

Fig. 4.4 Stress distribution (ST-2)

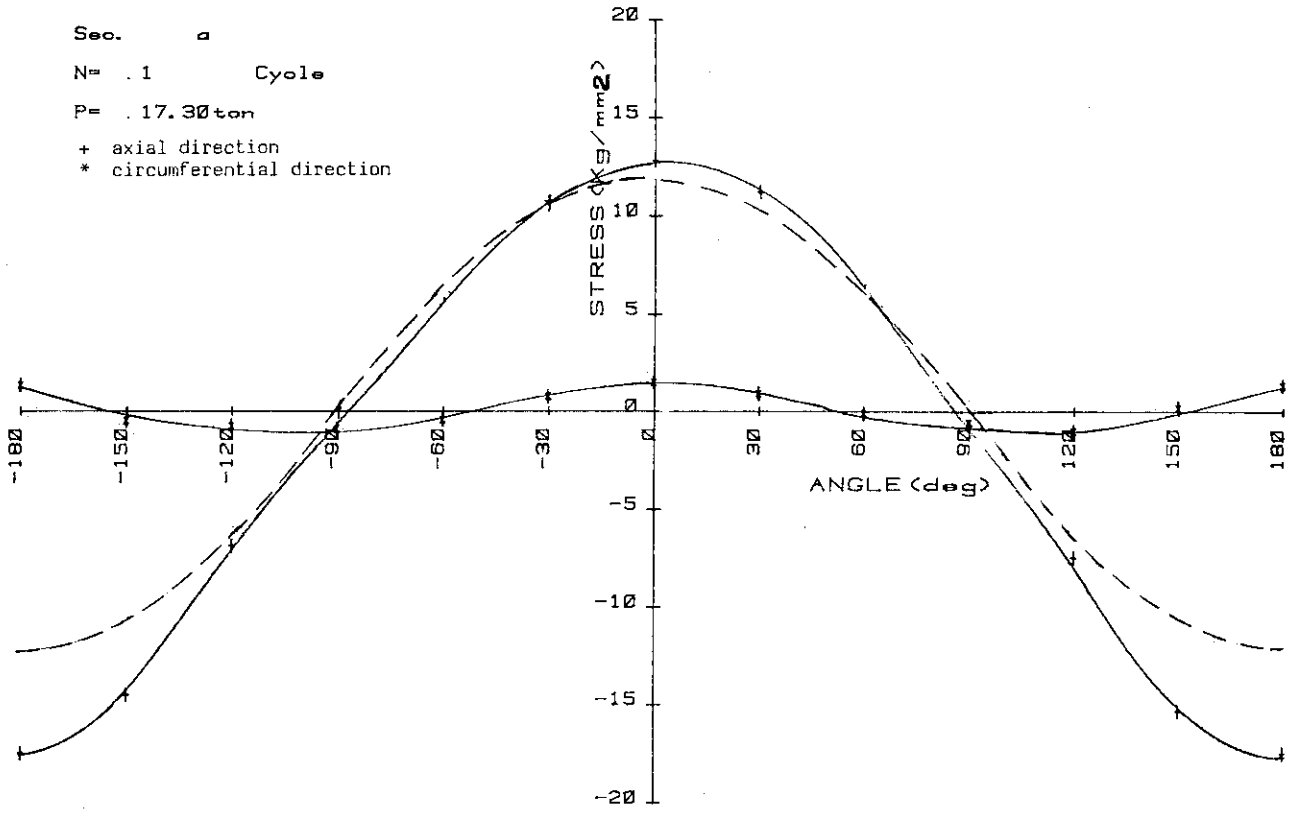

Fig. 4.5 Stress distribution (ST-2)

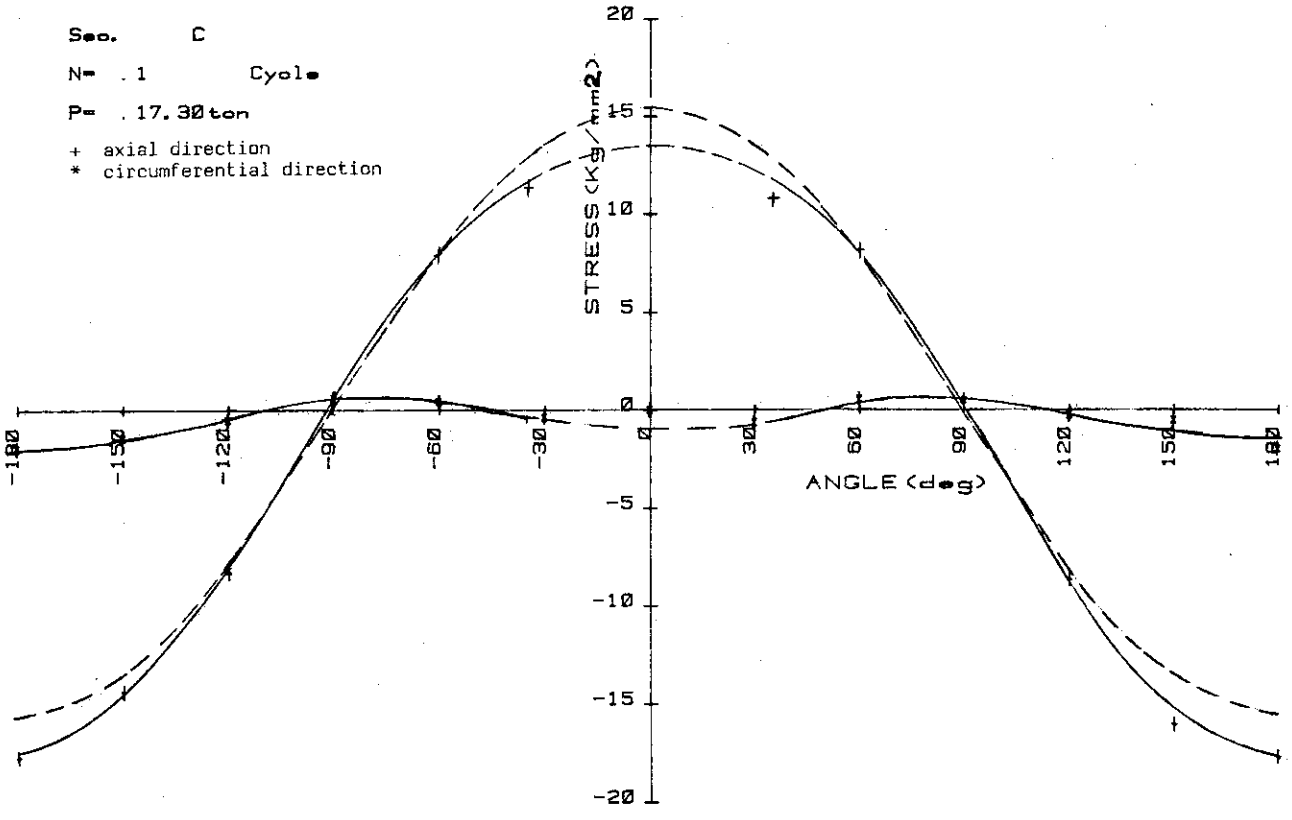

Fig. 4.6 Stress distribution (ST-2)

5. Fatigue test results

5.1 Fatigue crack growth measurements

The fatigue test had been performed till the crack passed through thickness and the crack length was less than 10 mm in the outer surface.

After the fatigue and fracture test were implemented, the test section was cut out from the test pipe, and the fracture surfaces were divided by a hydraulic machine for observation of the fracture surface.

Photos.5.1 and 5.2 show the fracture surface of ST-1 and ST-2 test pipe. The crack front marks of the fracture surface of ST-1 test pipe can be observed clearly, while those of ST-2 test pipe are not so clear.

However the crack depth and shape in the fracture surface of ST-2 test pipe could be almost recognized from the crack front marks obtained by the fatigue test. The appearances of the fracture surface are schematically depicted from their observation as shown in Figs.5.1 and 5.2.

The following notices are obtained from the fatigue test results of ST-1 test pipe.

The growth of C2 crack was most remarkable and C2 crack passed through the thickness. The crack initiated at the deepest point of the artificial defects, and crack front grew almost semi-circularly.

The crack front in the vicinity of the inner surface had a singular geometry, i.e., a convex shape, and there some delay of crack growth was always observed. This phenomenon seems to be caused by a difference of the stress state between the vicinity of the inner surface and the inside.

Though the cracks did not grow to the exact symmetrical configuration, a large single internal crack was realized at the end of the fatigue tests as expected before the test.

The crack growth behavior of ST-2 test pipe was different from that of ST-1 test pipe as it was observed in those test results.

In the test of ST-2 test pipe, cracks initiated in order of C1, C3 and C2, and grew larger cracks in the same order. The crack penetration was caused at C3 after the coalescence of three cracks. As the crack extension of ST-2 test pipe in the circumferential direction is

larger than that of ST-1 test pipe, the crack length of ST-2 test pipe is larger than that of ST-1 at the end of the fatigue test.

It seems that the above difference between crack growth behavior of ST-1 and ST-2 test pipes might be caused by the difference of the following test conditions:

(1) As the weld beads of ST-2 test pipe exists close to the test section, the geometry and the stress distribution in the test section is different from that of ST-1 test pipe.

(2) The cracks grow through the heat affected zone of the weldment, so that the crack growth behavior might be influenced by the change of the material properties.

(3) The crack growth behavior might be influenced by the residual stress caused during welding.

Three crack growth measuring techniques had been used during the fatigue test as described before.

Figs.5.3 and 5.4 show the crack depth obtained by the ultrasonic technique and by the fracture surface observation. The test results obtained by the ultrasonic technique give slightly smaller than those of the fracture surface observation, as shown in these figures. However it seems that the deviation of both the results is very small and the ultrasonic technique gives high accuracy.

In case of ST-2 test pipe, a particular crack growth behavior that C1 and C3 cracks grew faster than C2 is observed as shown in Fig.5.2 and Photo.5.2. The deepest points of C1 and C3 cracks tend to move from the center line of the artificial crack to C2 crack. The crack growth curves of ST-2 test pipe along the deepest point and the centerline (90° direction) are shown in Fig.5.5.

The crack growth curves of the ST-1 test pipe along the deepest point of C1 and C3 coincide almost with those along the centerline.

When the cracks approach the outer surface, the crack growth is very steep in both C2 of ST-1 and C1 of ST-2.

As the third method electric potential technique was used, this technique is not accurate enough to measure each crack depth, but only the behavior of the crack coalescence was measured accurately by it.

Figs.5.6 and 5.7 show the results of electric potential measurement. In these figures, No.2 and No.5 probes attached at the center between two cracks (No.2 probe at the center between C1 and C2 and No.4 probe at the center between C2 and C3), show steep electric potential

increase at certain cycles. It is because crack coalescences were caused around the point of electric potential increase.

From these figures and the fracture surface observation the point of the crack coalescence can be estimated accurately. These estimated results are shown in Table 5.1.

5.2 Crack growth rate

The crack growth rate of each crack of ST-1 test pipe along the radial direction was obtained from the beach mark spacing. Fig.5.8 shows the relationship between da/dN and crack depth, a, of each crack. As shown in this figure, each curve shows good agreement till the cracks grow to the depth of 18 mm, and the difference is caused among three curves when they are closer with growth of each crack front in the inner surface.

From the experimental results, it seems that each crack growth behavior is likely to be a single independent crack before they grow to a large crack and are close mutually.

The influence of the crack coalescence on da/dN vs. a curves seems to be the largest for C1 crack, because the crack growth rate of C1 crack is larger than that of C2 and C3 cracks and they have almost the same crack growth rate as shown in Fig.5.8.

As shown in Fig.5.9, the relationship between da/dN and the crack depth, a, of ST-2 test pipe is somewhat different from that of ST-1. As shown in Fig.5.2, the crack growth of C1 and C3 cracks is larger than that of C2 crack. Consequently the crack growth behavior of ST-2 test pipe is different from that of ST-1 after three cracks coalesce.

The curves of da/dN vs. crack depth in the smallest cracks of both the test pipes show the steepest increase. It means that the effect of coalescence on the crack growth rate of the smallest crack is larger than that of larger cracks. It is assumed that the stress concentration in the vicinity of the smallest crack is caused, due to the geometrical effect of the coalesced crack.

5.3 comparison of crack growth

An analytical procedures for evaluation of the flaws detected in the in-service inspection of the structural components and the criteria

for acceptability of the flaws are specified for preventing the brittle fracture based on the fracture mechanics in the Section XI of ASME Boiler and Pressure Vessel code[2]. This analytical procedures were applied to evaluate the crack growth of ST-1 and ST-2 test pipes and both the results were compared.

The analytical procedures are outlined as follows:

(1) Modification of the cracked structure to apply the procedures.

(2) Determination of the stress intensity factor for simplified models.

(3) Determination of the incremental flaw growth, Δa (a = minor half diameter of a semi-elliptical crack), corresponding to ΔN load cycles, using ΔK of the model and da/dN vs. ΔK relationship of the material.

(4) Determination of the incremental flaw growth, Δb (b = major half diameter of a semi-elliptical crack), assuming that the similar configuration is kept during the crack growth.

(5) Updating of the crack by calculating $a + \Delta a$ and $b + \Delta b$ and alternating the procedures.
When the multiple cracks satisfy the crack coelescence criteria, they are regarded as a single crack according to the procedures.

Main specifications of the analytical models for ST-1 and ST-2 test pipes are shown in Table 5.2. The analysis has been performed using the actual dimensions and load conditions, which are slightly different from the values specified by JIS.

The analytical model is an infinite flat plate with cracks and is subject to uniform tension and bending moment. Analytical models and the condition of the crack coalescence in detail are illustrated in Fig.5.10, and the material crack growth characteristic (da/dN vs. ΔK curve) used in the analysis is shown in Fig.5.11. The upper and lower curves in Fig.5.11 have been used.

The stress intensity range, ΔK, was obtained from the following equation[2]:

$$\Delta K = \sqrt{\frac{\pi a}{Q}} \left(\Delta\sigma_m M_m + \Delta\sigma_b M_b \right)$$

The analysis has been performed on the flaw depth to thickness ratio from 0.25 to 0.5 because M_b value is available to the ratio, $a/t = 0.5$,

in the ASME Code[2]. The analytical results are compared with experimental results as shown in Fig.5.12.

The analytical results of ST-1 and ST-2 test pipes give a conservative evaluation for the crack growth life. The break point occurs in the analytical curves as shown in Fig.5.12 and indicates the crack coalescence of three cracks, and a jump of the crack length and ΔK value occurs here resulting in very steep crack growth. Meanwhile it is known from the test results that the cracks grow in more circular configuration and the crack aspect ratio, a/b, is not kept to be 0.67 of the initial value, and consequently crack coalescence is caused at a deeper point of the cracks than those expected analytically.

Besides no drastic change in the crack growth curve after the crack coalescence is seen in the experimental curves, and when cracks coalesce, they are not large enough to regard as a large single crack at the crack coalescence.

Therefore the criteria of the crack coalescence specified in the ASME code is too conservative for the same crack geometry, $a/b = 0.67$, as in these tests.

The test of ST-2 test pipe was performed on the heat affected zone of the weldment. In this case the crack coalescence is caused earlier than ST-1 test pipe as shown in Fig.5.12. It is because the crack growth to the circumferential direction of ST-2 test pipe is much larger than that of ST-1 test pipe. And this fact suggests a possibility that the crack of heat affected zone grows more wide and shallow than that of base metal.

Table 5.1 Crack depth and number of cycles at the crack coalescences

	location of coalescence	a_1 mm	a_2 mm	a_3 mm	N cycle
No.1 Test pipe	C2 - C3	19.6	27.4	22.7	620,000
	C1 - C2	21.0	30.4	25.0	640,000
No.2 Test pipe	C1 - C2	17.0	12.2	15.7	420,000
	C2 - C3	20.7 (19.9)*	14.5	18.5 (18.2)*	530,000

* ( ): crack depth of 90° direction

Table 5.2 Specification of analyzed model

Items		ST-1 pipe model	ST-2 pipe model
thickness,	t mm	35.0	32.3
outer diam.,	D_o mm	320.0	320.0
inner diam.,	D_i mm	250.0	255.4
moment of inertia,	I mm^4	3.23×10^8	3.06×10^8
section modulus,	Z mm^3	2.02×10^6	1.91×10^6
moment load,	ΔM ton-m	26.8	26.8
stress range,	$\Delta\sigma$ kg/mm^2	13.3	14.0
manbrane stress range (primary),	$\Delta\sigma_m$ kg/mm^2	11.8	12.6
bending stress range (primary),	$\Delta\sigma_b$ kg/mm^2	-1.4	-1.4
0.2% yield strength,	σ_{YS} kg/mm^2	28.0	28.0

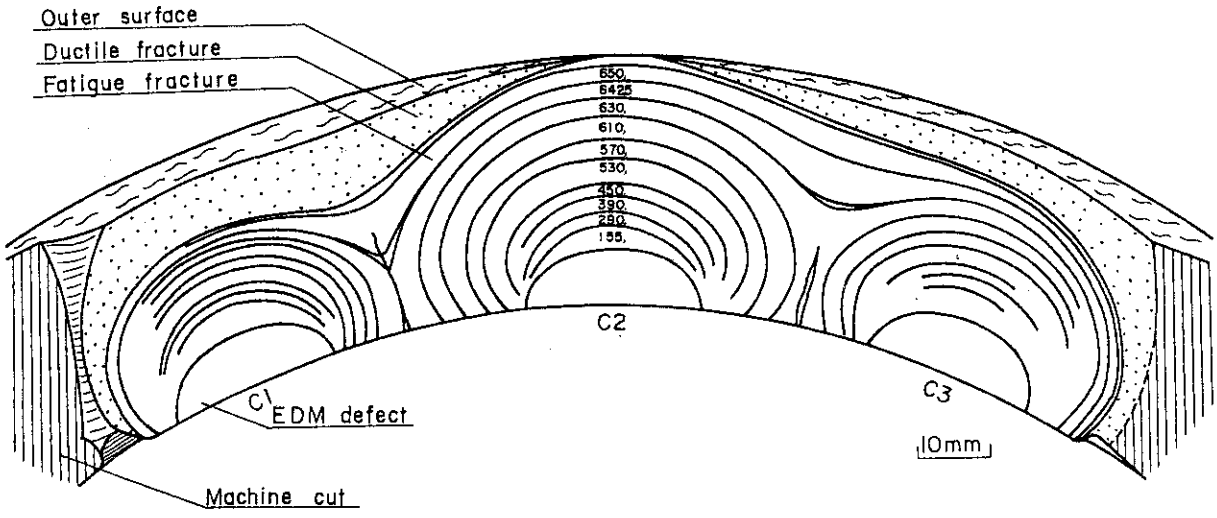

Fig. 5.1 Fracture surface appearance of ST-1 test pipe

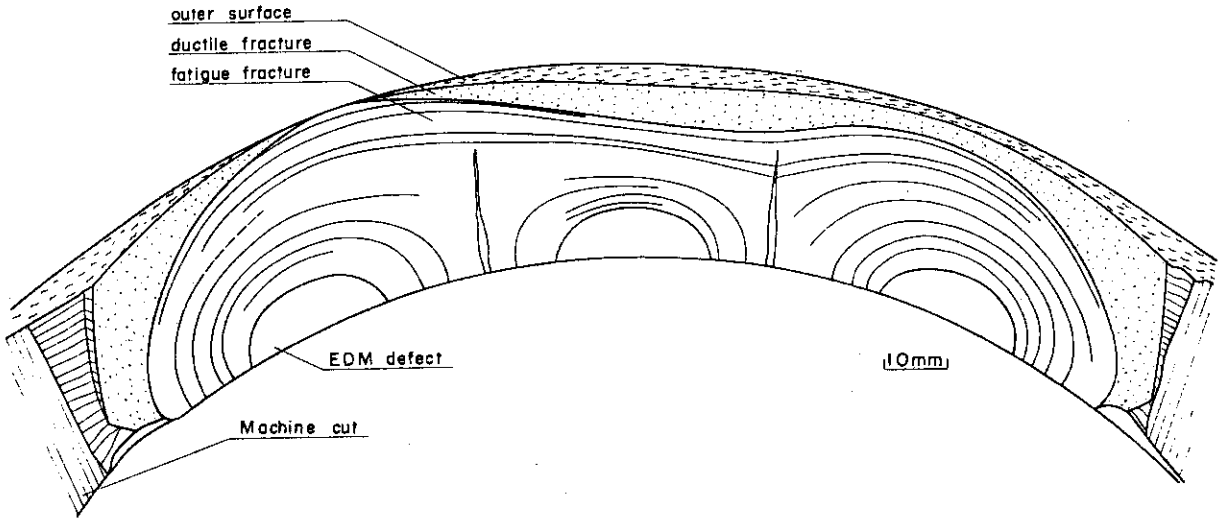

Fig. 5.2 Fracture surface appearance of ST-2 test pipe

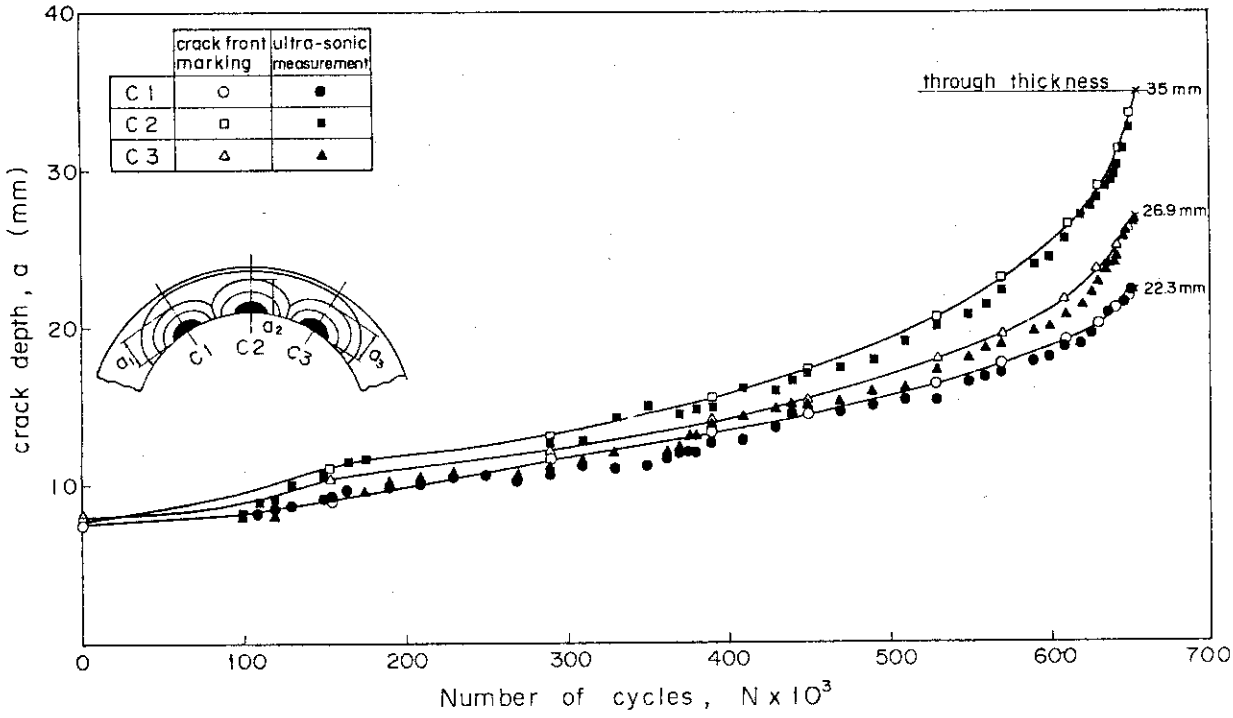

Fig. 5.3 Crack depth vs. N curves of ST-1 test results

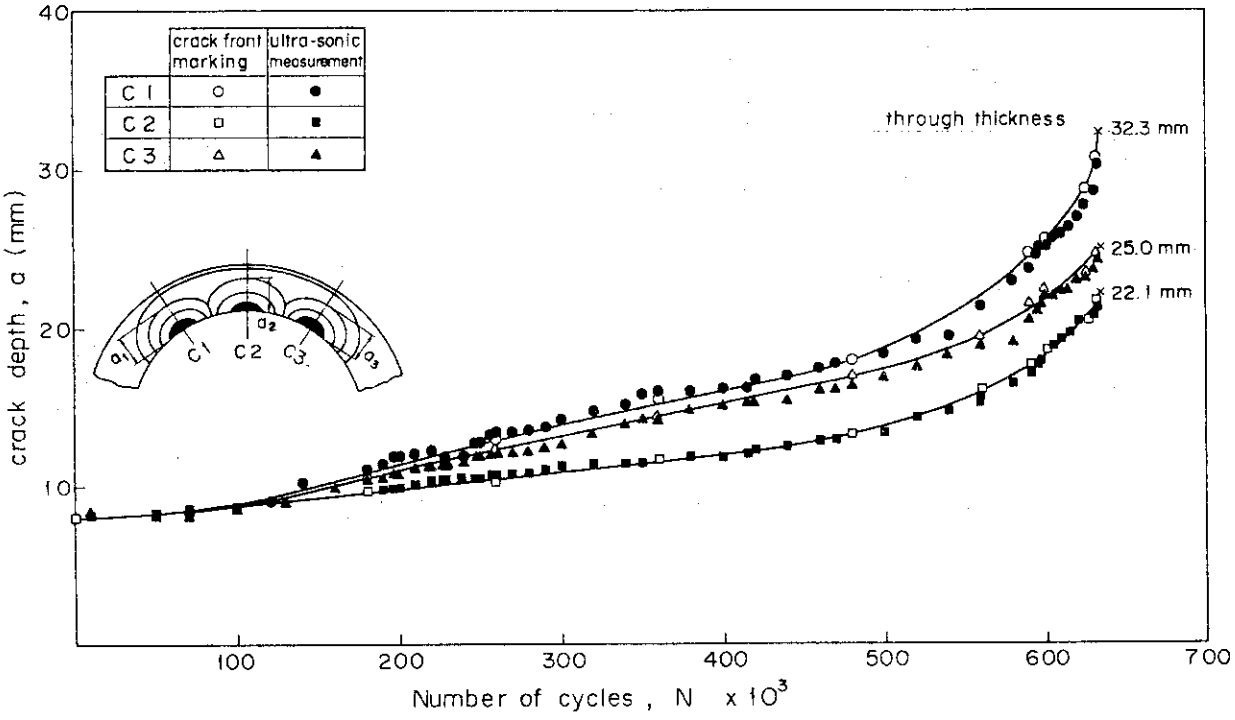

Fig. 5.4 Crack depth vs. N curves of ST-2 test results

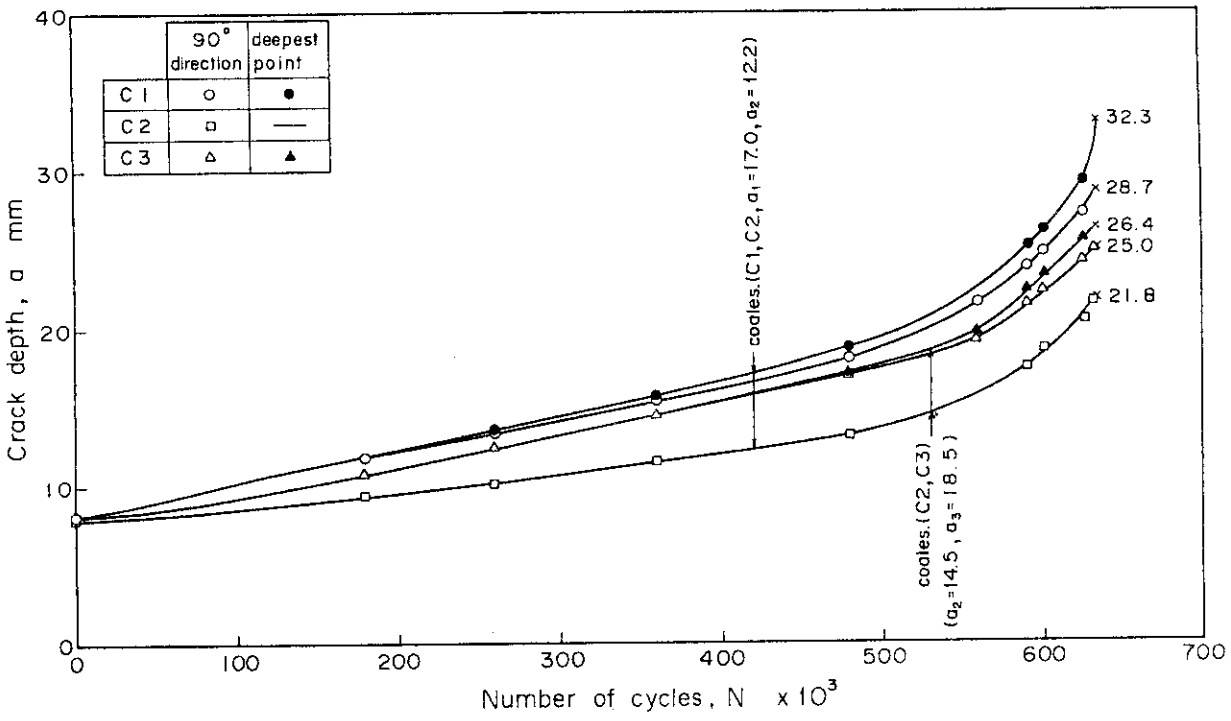

Fig. 5.5 Summary of crack depth vs. N curve obtained by fracture surface observation

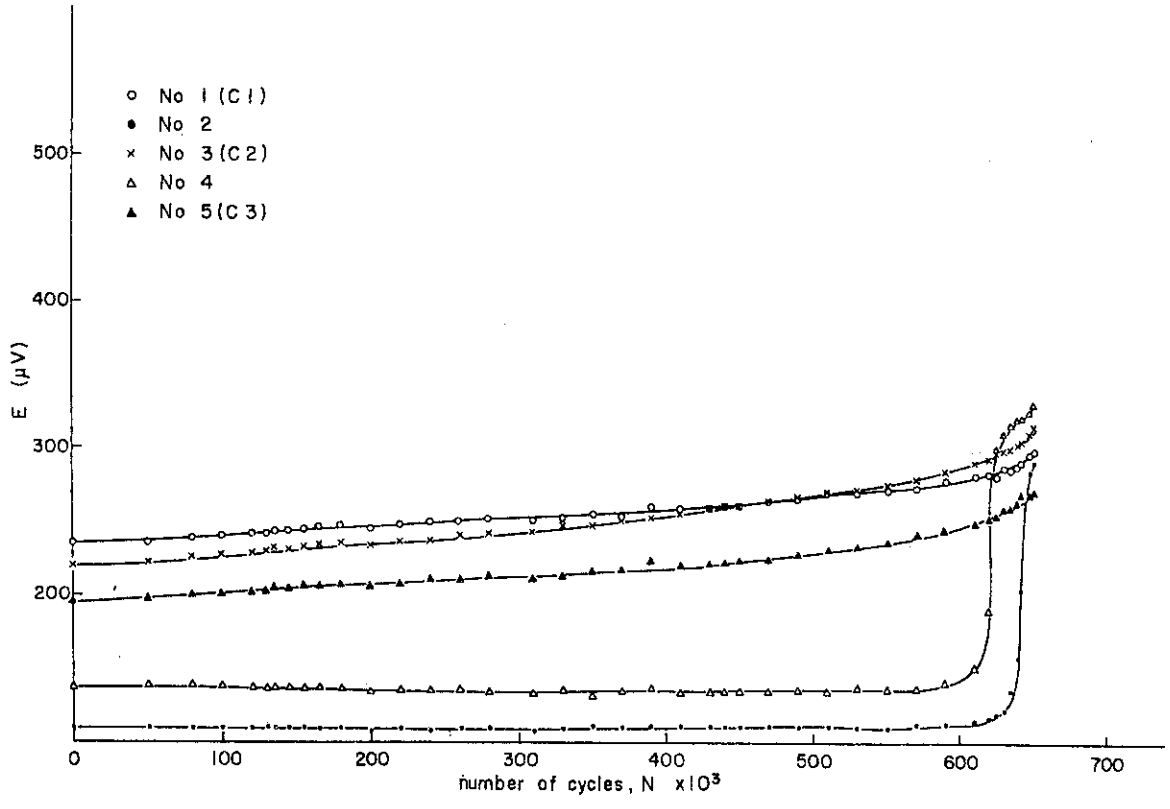

Fig. 5.6 Results of electric potential measurement (ST-1)

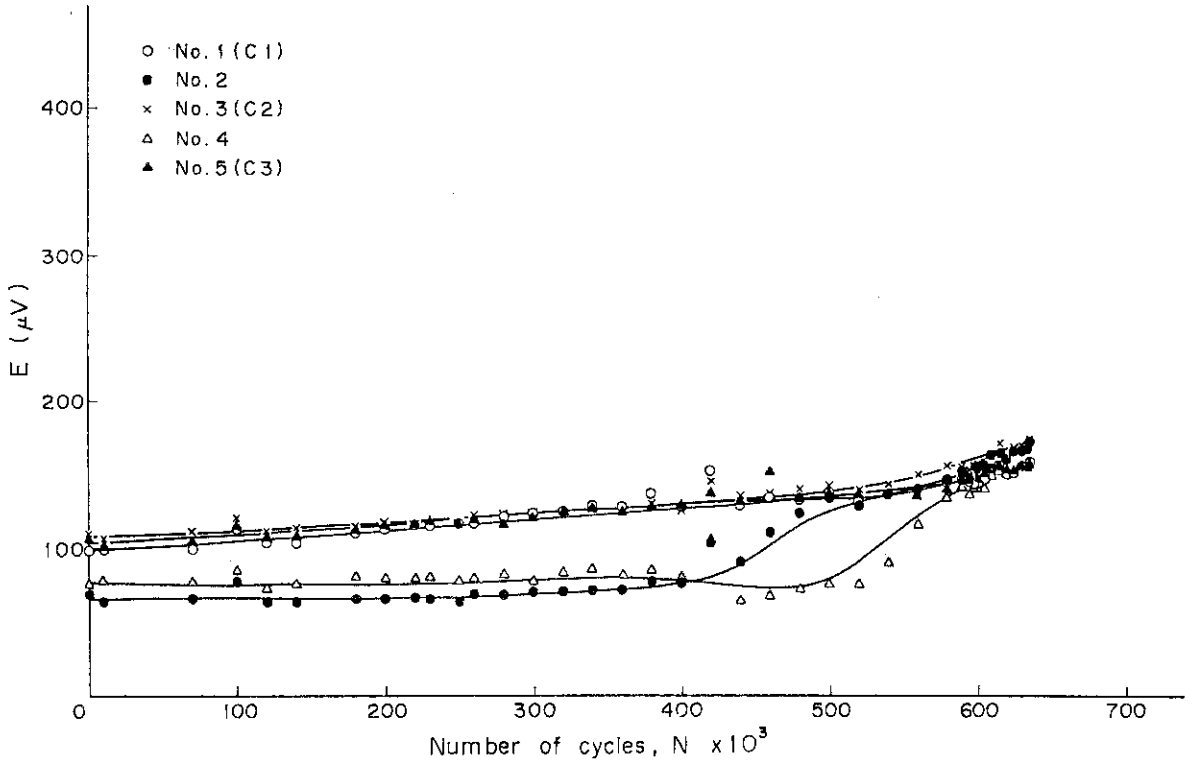

Fig. 5.7 Results of electric potential measurement (ST-2)

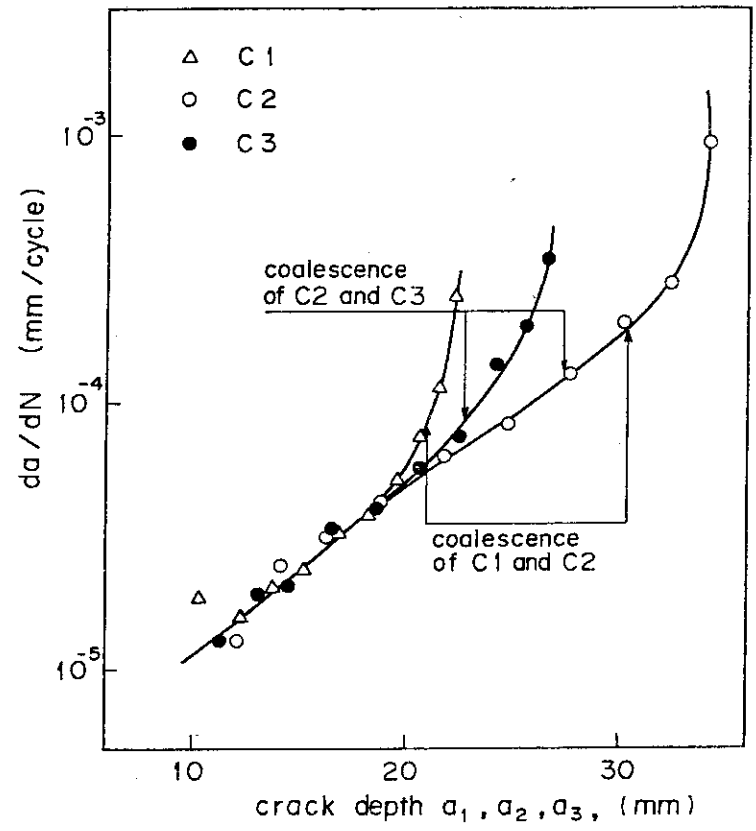

Fig. 5.8 da/dN vs. a curue (ST-1)

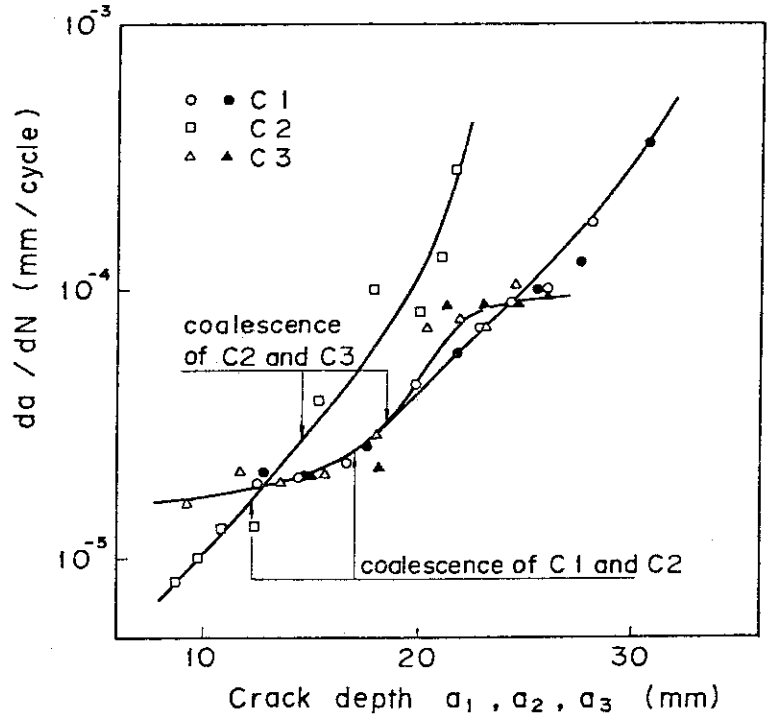

Fig. 5.9 da/dN vs. a curve (ST-2)

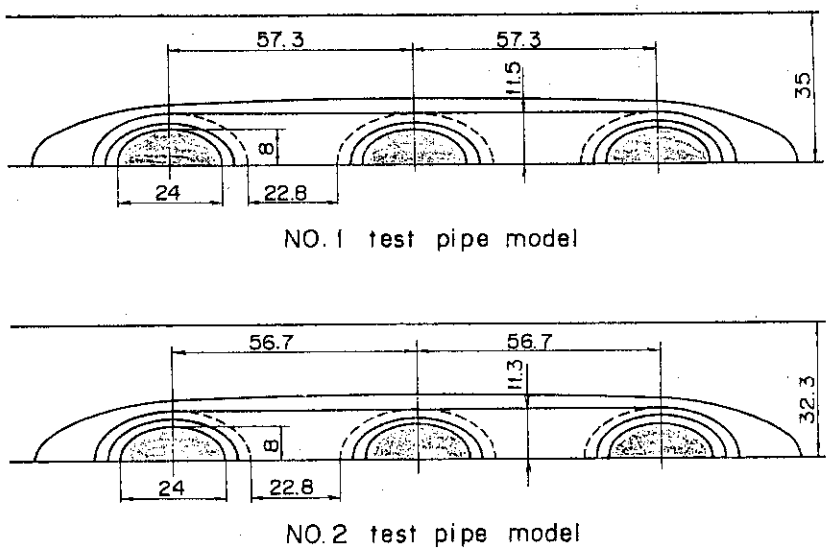

Fig. 5.10 Analized model of NO.1 and NO.2 test pipe

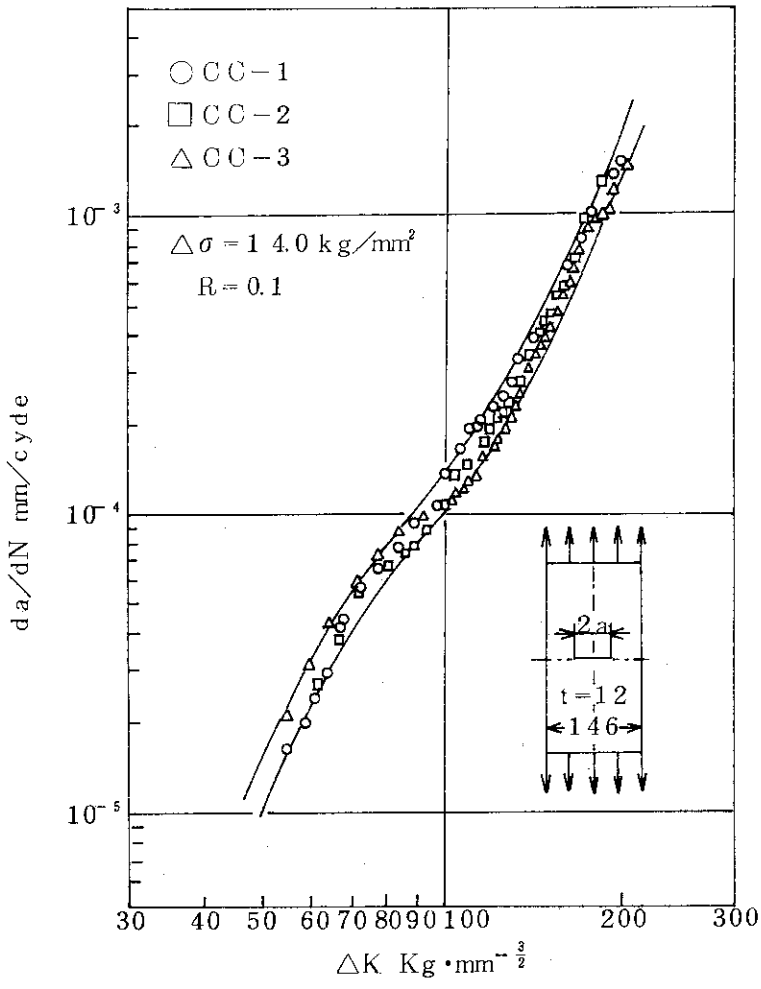

Fig. 5.11 Relationship between da/dN and ΔK for tested pipe material

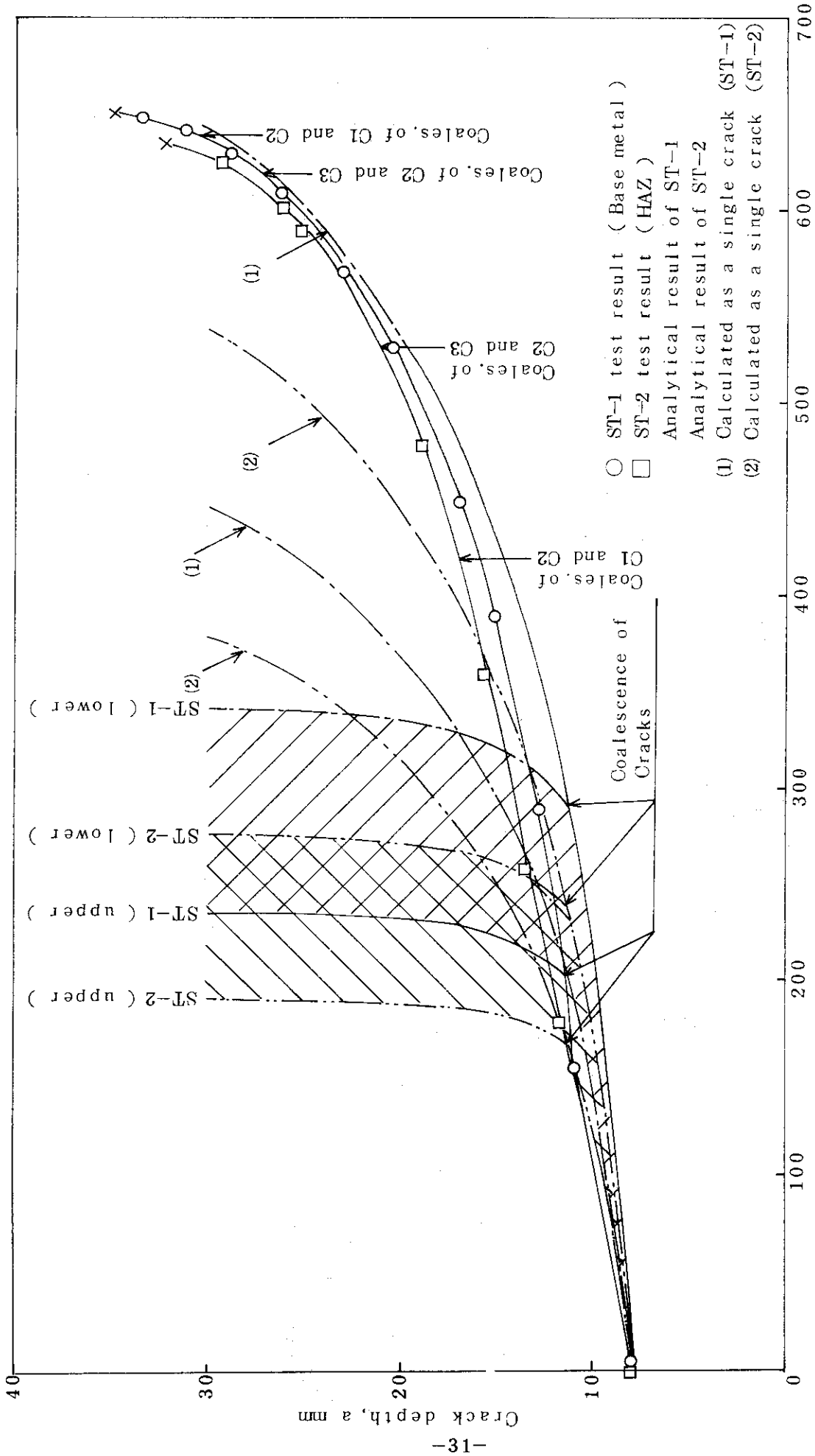

Fig. 5. 12 Comparison of crack depth vs. N curve between analytical and tested results

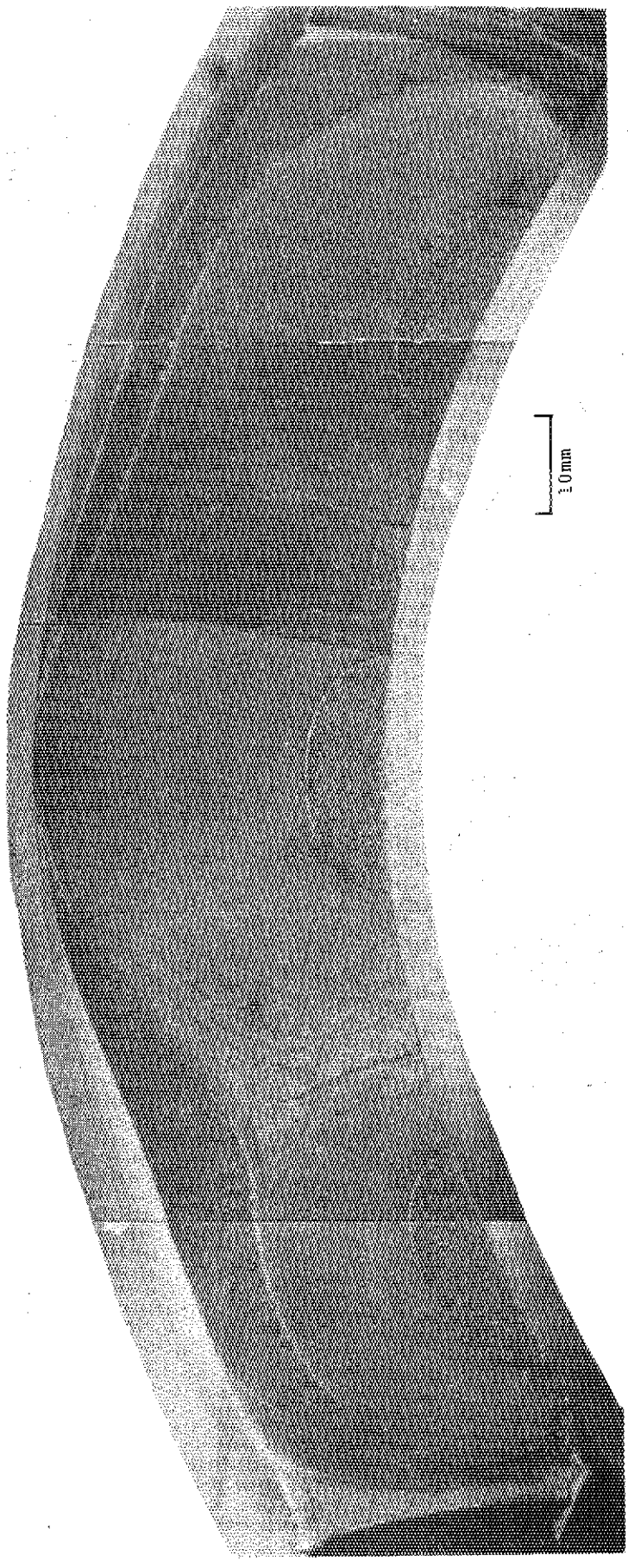

Photo. 5.1 Fracture surface appearance of the No.1 test pipe

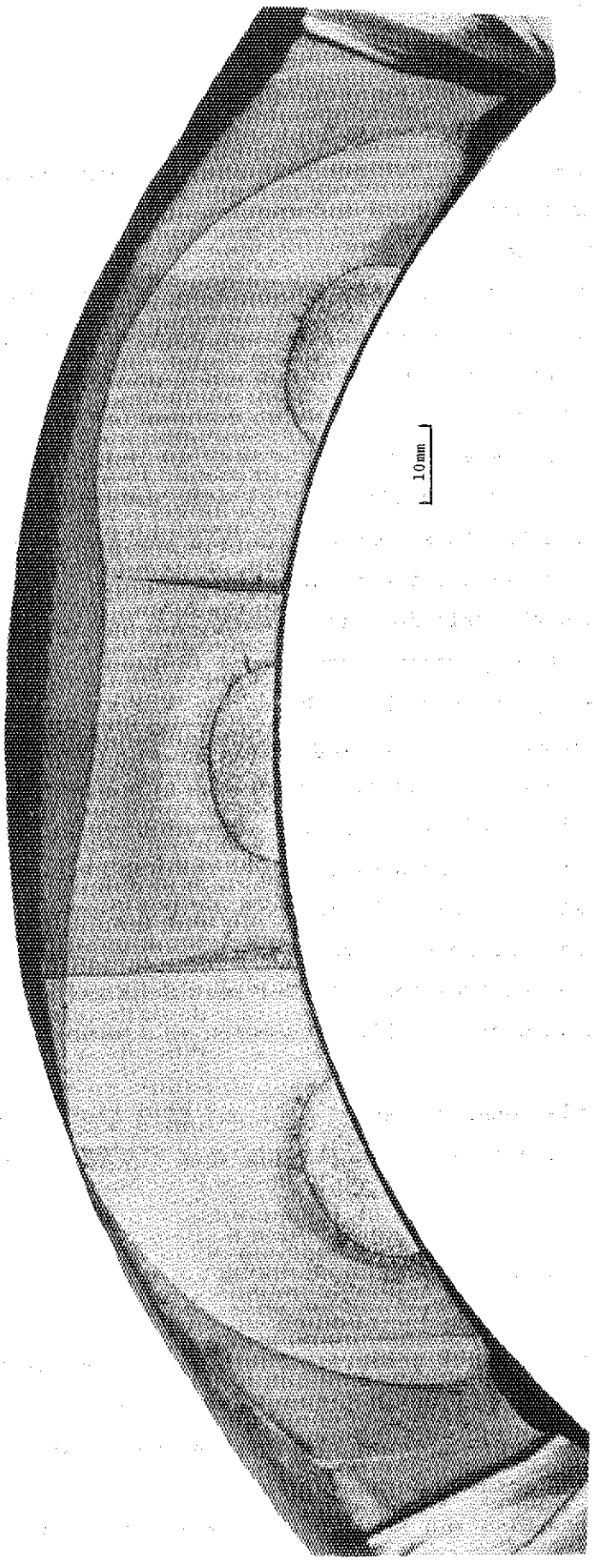

Photo. 5.2 Fracture surface appearance of the No.2 test pipe

6. Fracture test results

6.1 Results of strain and displacement measurement

Following the fatigue test, a fracture test was performed by an overload under displacement control, and deformation and crack extention behavior were investigated.

Figs.6.1 to 6.6 show the relationship between load and strains in the vicinity of the crack. It is observed in these figures that the test pipe exhibits an elastic behavior to 30 ton and gradual increase of a plastic deformation to 40 ton. The plastic deformation of ST-1 and ST-2 test pipes increases steeply with load over 40 ton, and noticeable crack extension is caused with this plastic deformation as shown later. Therefore the fracture mode of the test pipes reveals ductile fracture accompanied with large plastic deformation.

Figs.6.7 and 6.8 show the relationship between load and displacement of the gage (D4) and the hydraulic actuater of ST-1 test pipe. It is evident from these figures that both the curves are almost identical and the deformation of the loading apparatus is negligible.

The relationship between load and displacement of ST-2 test pipe is shown in Figs.6.9 and 6.10 and is almost the same as ST-1 as shown in these figures. However, there is a distinctive feature that the load decrease is caused slightly with the increase of displacement around $\delta = 80$ to 100 mm, and the load increases again. This behavior of ST-2 test pipe is different from that of ST-1 test pipe and the local load decrease is a kind of unstable phenomenon as discussed later.

These loads vs. displacement curves of ST-1 and ST-2 test pipes show a tendency that the load is still increasing when the displacement is more than 200 mm.

6.2 Results of crack extension measurement

In the fracture test the crack penetrated locally at the end of the fatigue test extends gradually to the circumferential direction at the outer surface of the test pipe. This crack extension was observed by photographs as shown in Photos.6.1 and 6.2.

The crack extension of ST-1 and ST-2 test pipes is noticeable

after 40 ton, and proceeds with the increase of plastic deformation as described before.

In case of ST-2 test pipe a secondary crack penetration is caused at the C3 side as shown in Photo.6.2. Subsequently two cracks extend to circumferential direction and coalesce in the outer surface. These crack extension and coalescence are caused while the applied load is locally decreasing. This means that an unstable crack extension is caused though it is quite local.

When the load is more than 45 ton, the crack extension is low, but the crack opening displacement is very high, as shown in Photo.6.2.

6.3 Summary of fracture test

In the fracture test the test pipes were loaded up to P = 49 ton (more than 200 mm of the actuater displacement), and unloaded due to limit of the actuater displacement. The relationship among loads, displacement and crack extension are summarized in Figs.6.11 and 6.12.

The crack extension of ST-1 and ST-2 test pipes was observed from P = 30 ton, and was high over 40 ton. The crack extension proceeds with plastic deformation, that is, it is known from strain measurement that the plastic deformation is caused before the crack extends, and the general yield of the test section is caused over 40 ton. Therefore the crack extension is accompanied with large plastic deformation.

The relationship between load and displacement of ST-2 test pipe shows the behavior that load decrease is caused at displacement, δ = 80 to 100 mm, whereas the crack extension is noticeable at this displacement and the coalescence of two cracks (C1 and C3) is caused at the outer surface. This unstable crack extension might have been caused due to the crack geometry at the end of the fatigue test of ST-2 test pipe. This means that a local unstable crack extension can be caused under certain geometrical condition though the fracture is grossly stable.

It is known from Fig.6.12 that the cracks coalesce in the outer surface and the crack becomes a large penetrated one over the displacement, δ = 100 mm. In this displacement the crack extension is low, whereas the increase of crack opening displacement is almost linear with the displacement, and the progress of deformation is very large. This behavior is almost the same with ST-1 test pipe. The load vs.

displacement curves of the ST-1 and ST-2 test pipes show a tendency that the load is still increasing when the displacement is more than 200 mm. Allowable load of the faulted condition defined in the Section III, Appendix F of ASME Code is 46.8 ton (3 S_m) for the test pipes, and the test results of ST-1 and ST-2 test pipes indicate that they have enough strength and toughness for this allowable load, even though a large crack exists in the inner surface of the pipe.

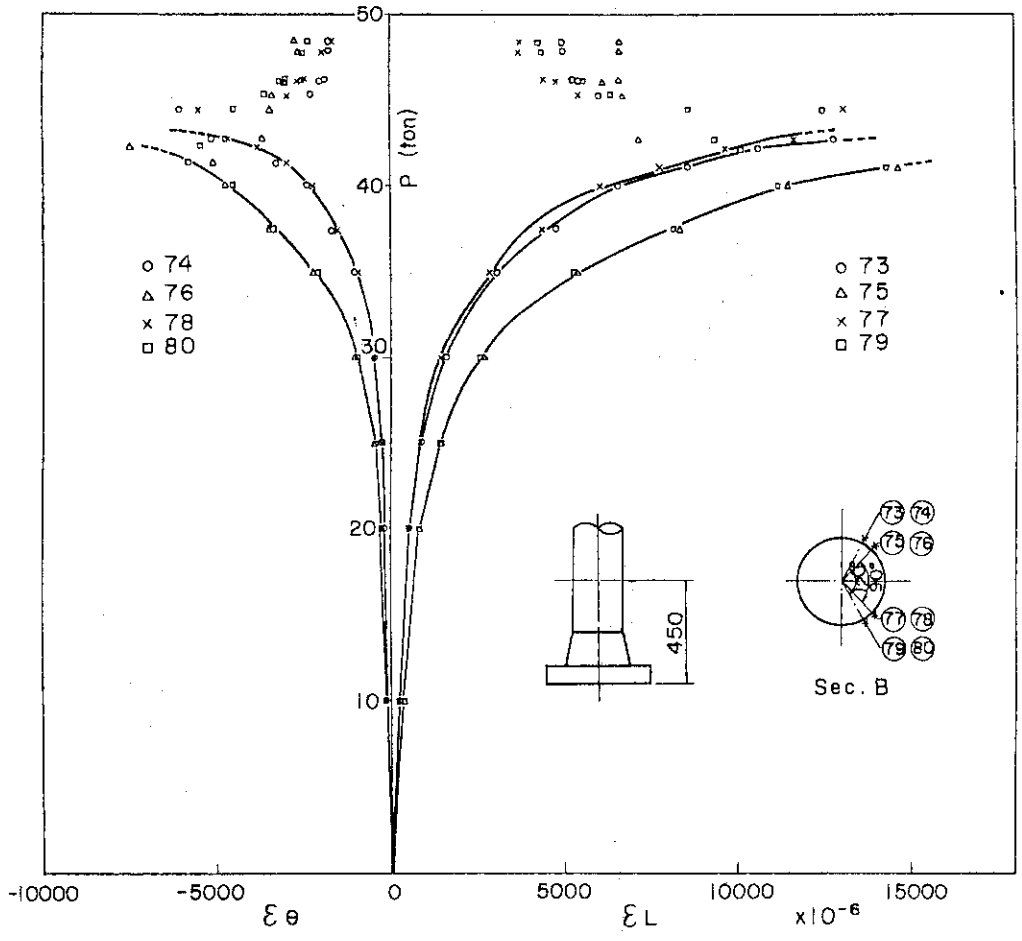

Fig. 6.1 Load vs. strain curve (ST-1)

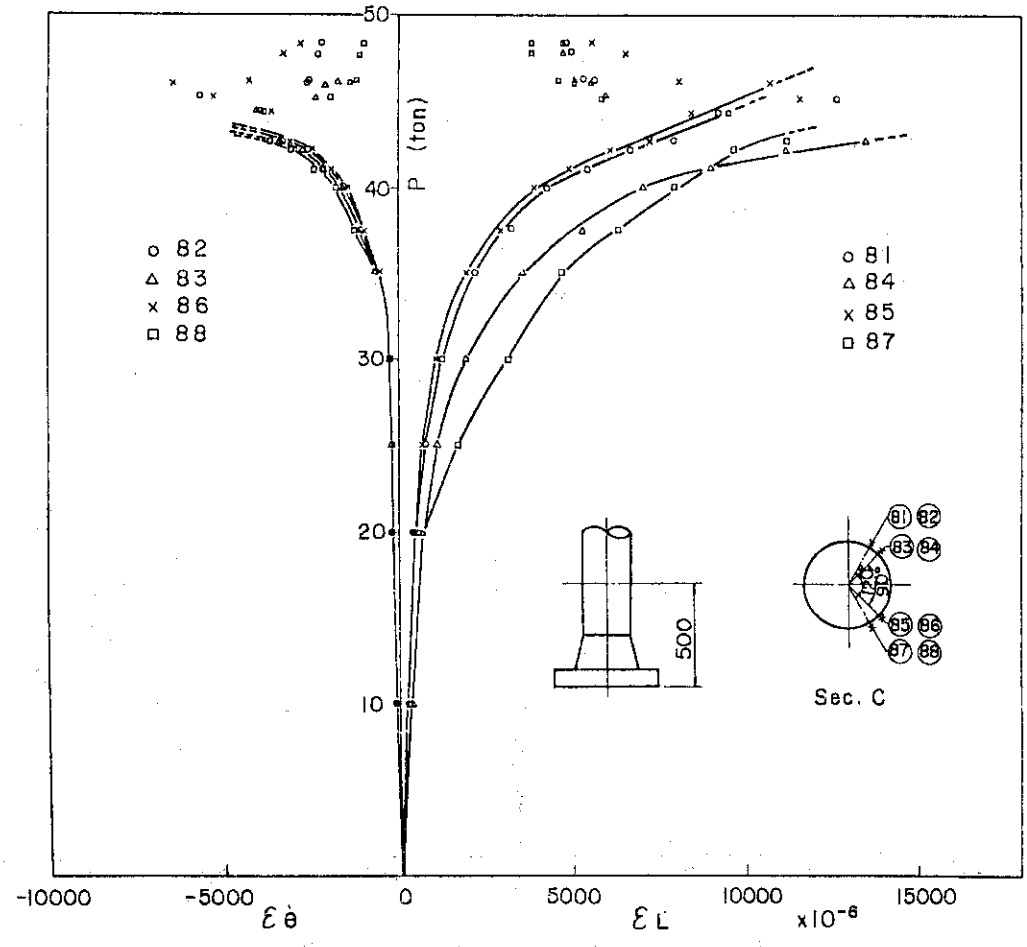

Fig. 6.2 Load vs. strain curve (ST-2)

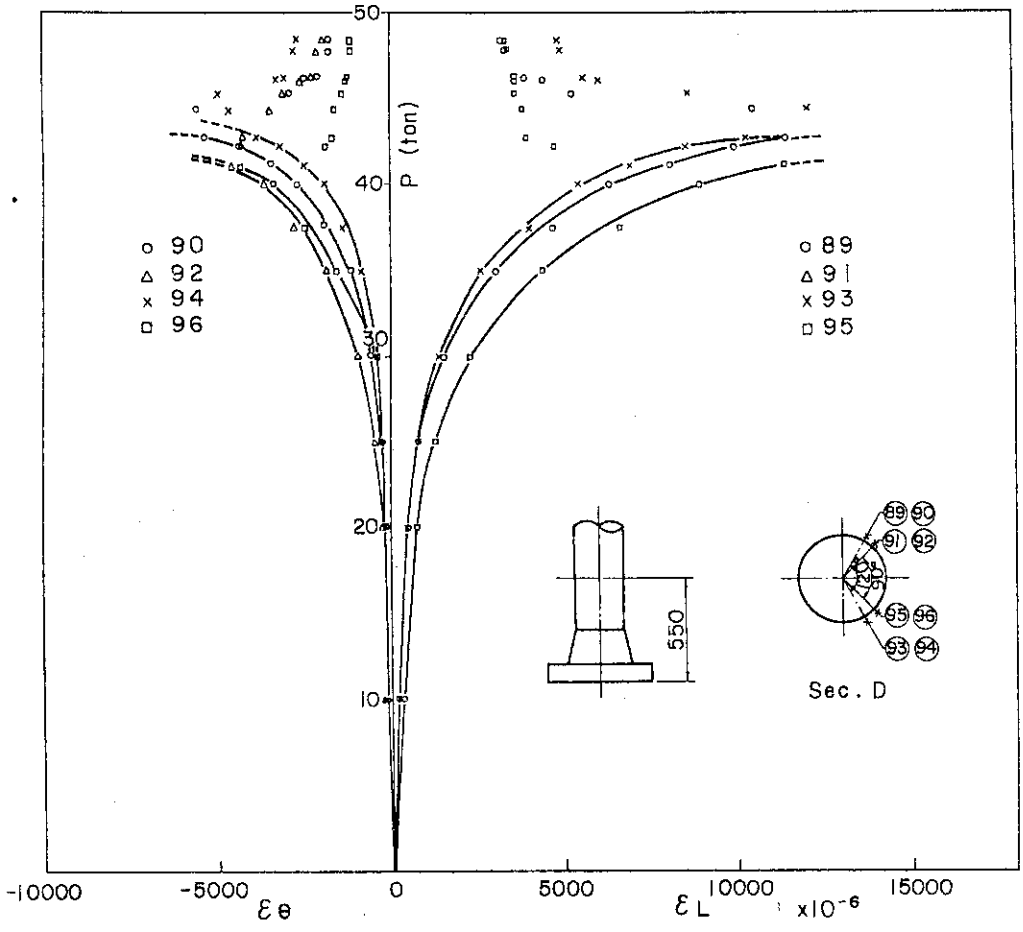

Fig. 6.3 Load vs. strain curve (ST-1)

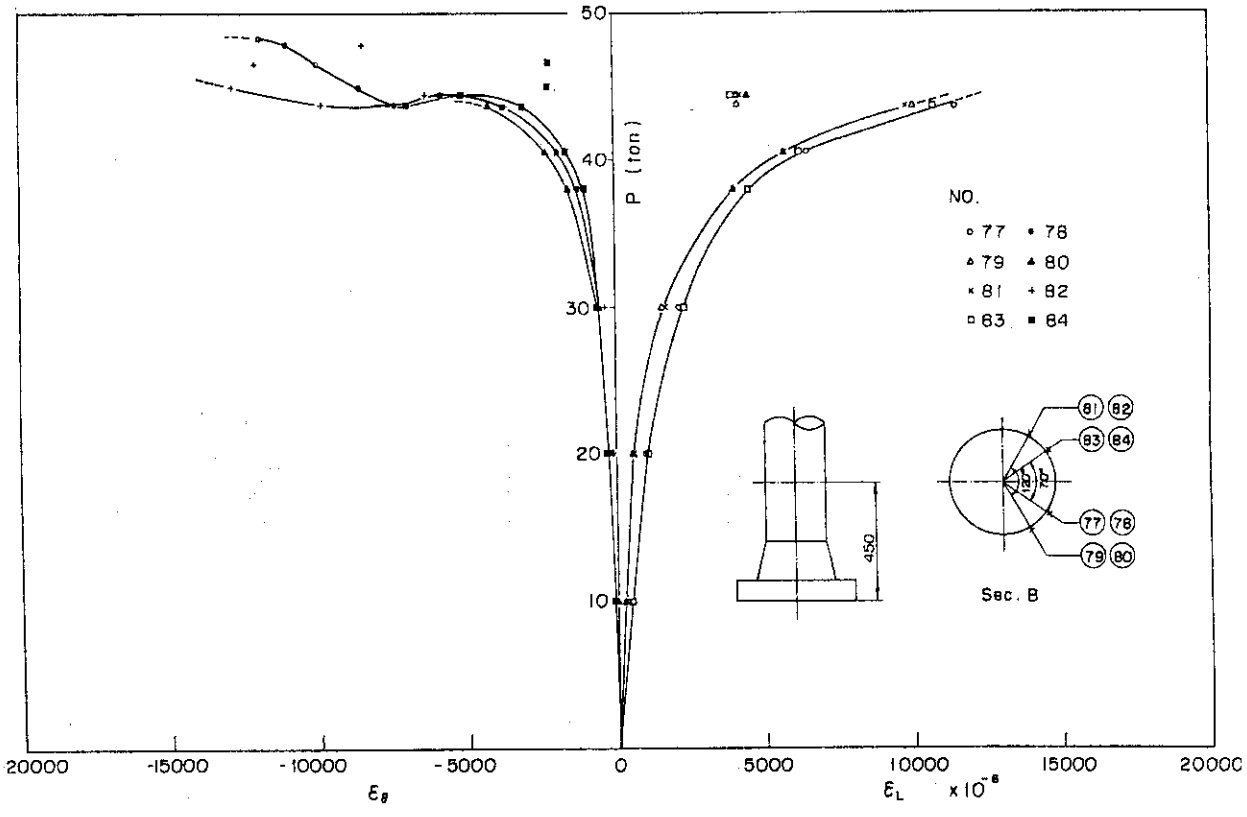

Fig. 6.4 Load vs. strain curve (ST-2)

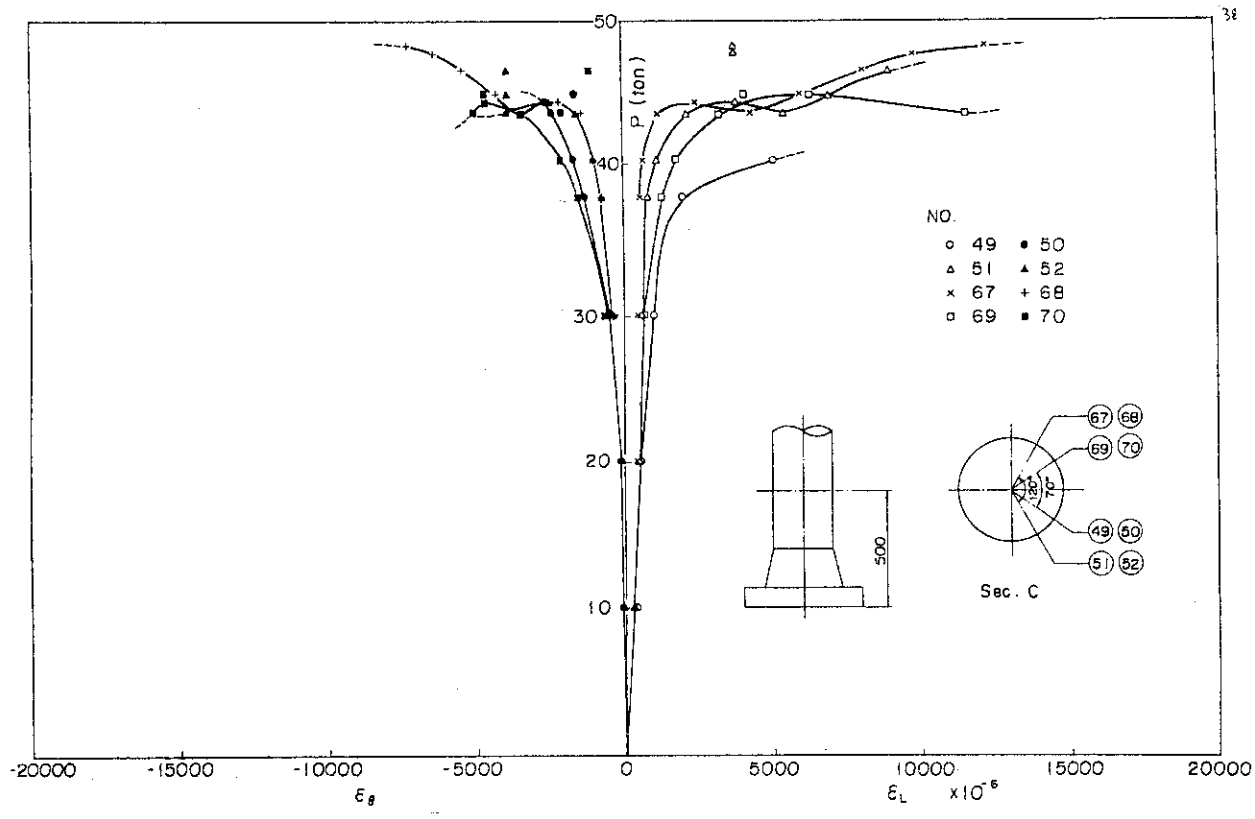

Fig. 6.5 Load vs. strain curve (ST-2)

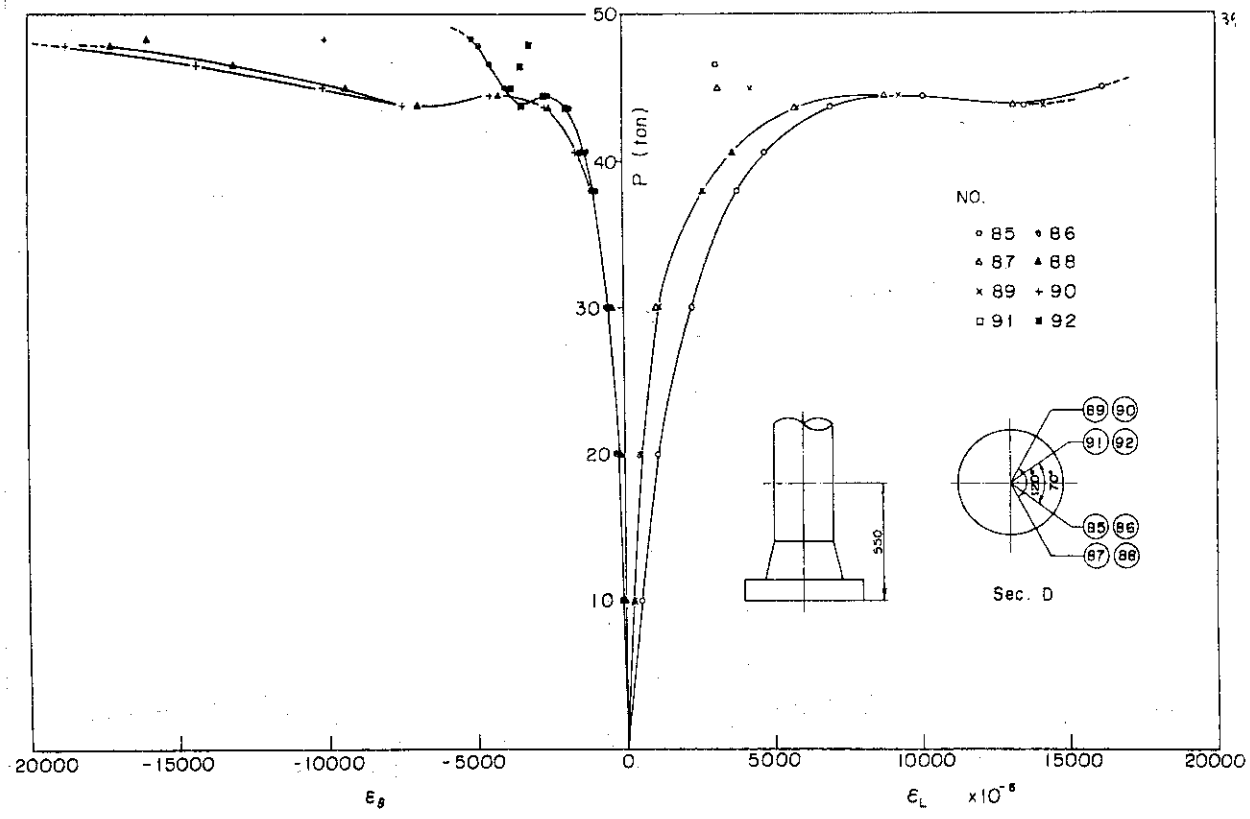

Fig. 6.6 Load vs. strain curve (ST-2)

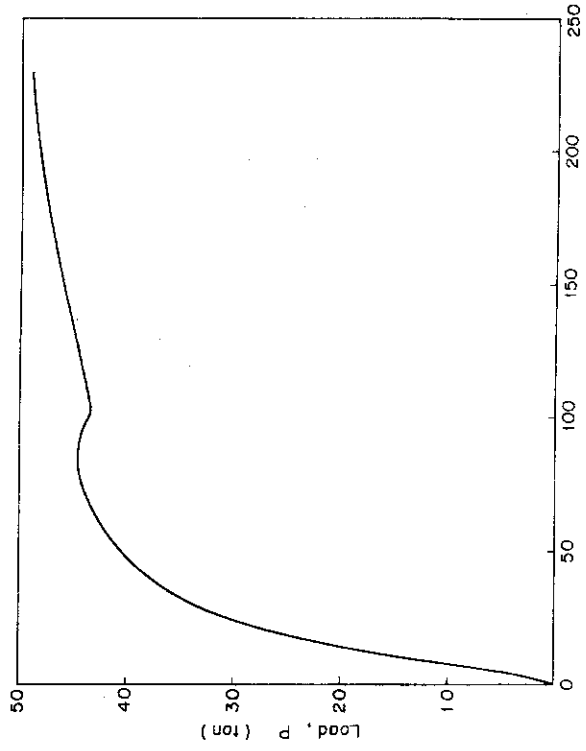

Fig. 6.7 Load vs. displacement curve (ST-1)

Fig. 6.9 Load vs. displacement curve (ST-2)

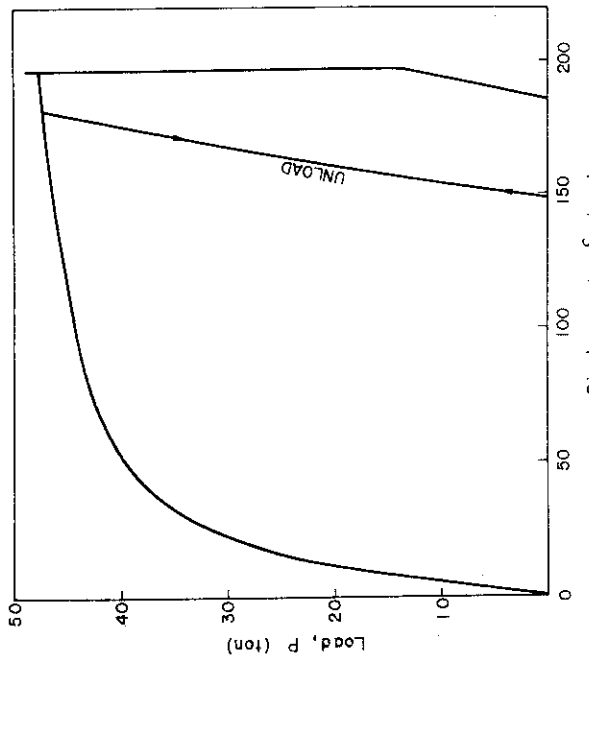

Fig. 6.8 Load vs. displacement curve (ST-1)

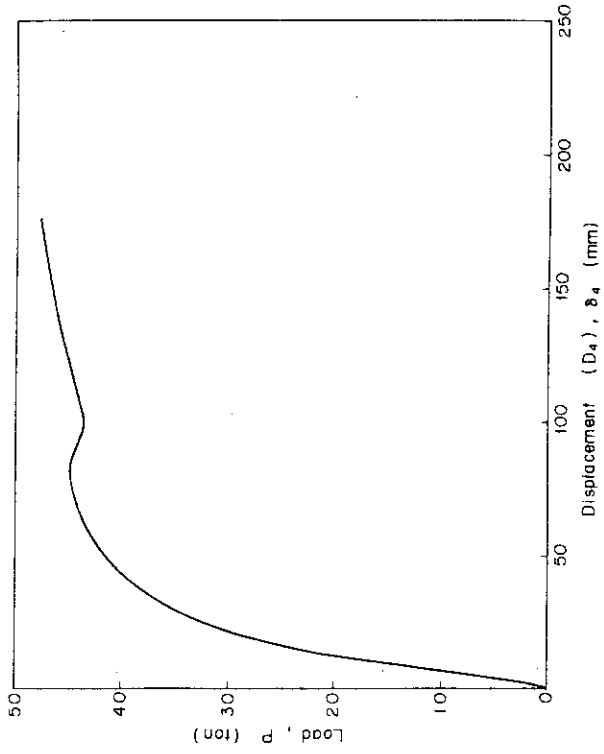

Fig. 6.10 Load vs. displacement curve (ST-2)

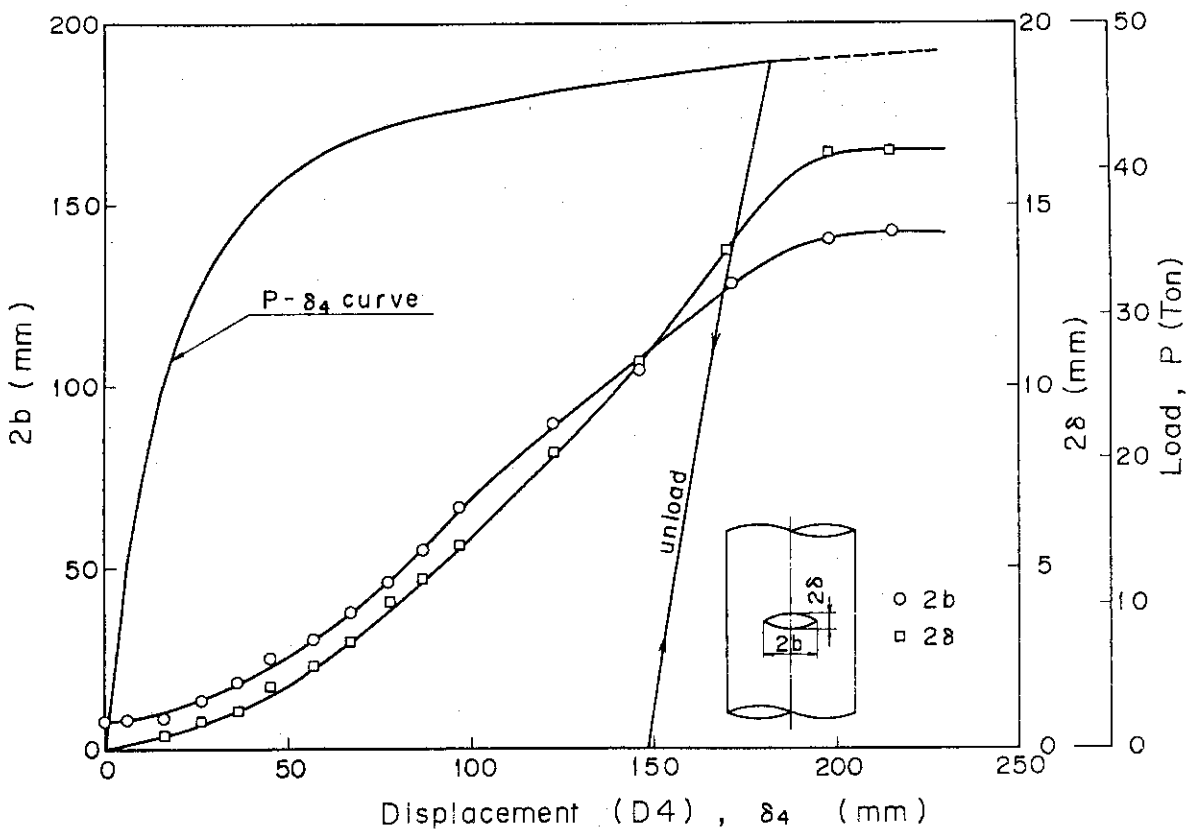

Fig. 6.11 Result of crack size and COD measurement of the outer surface in the fracture test

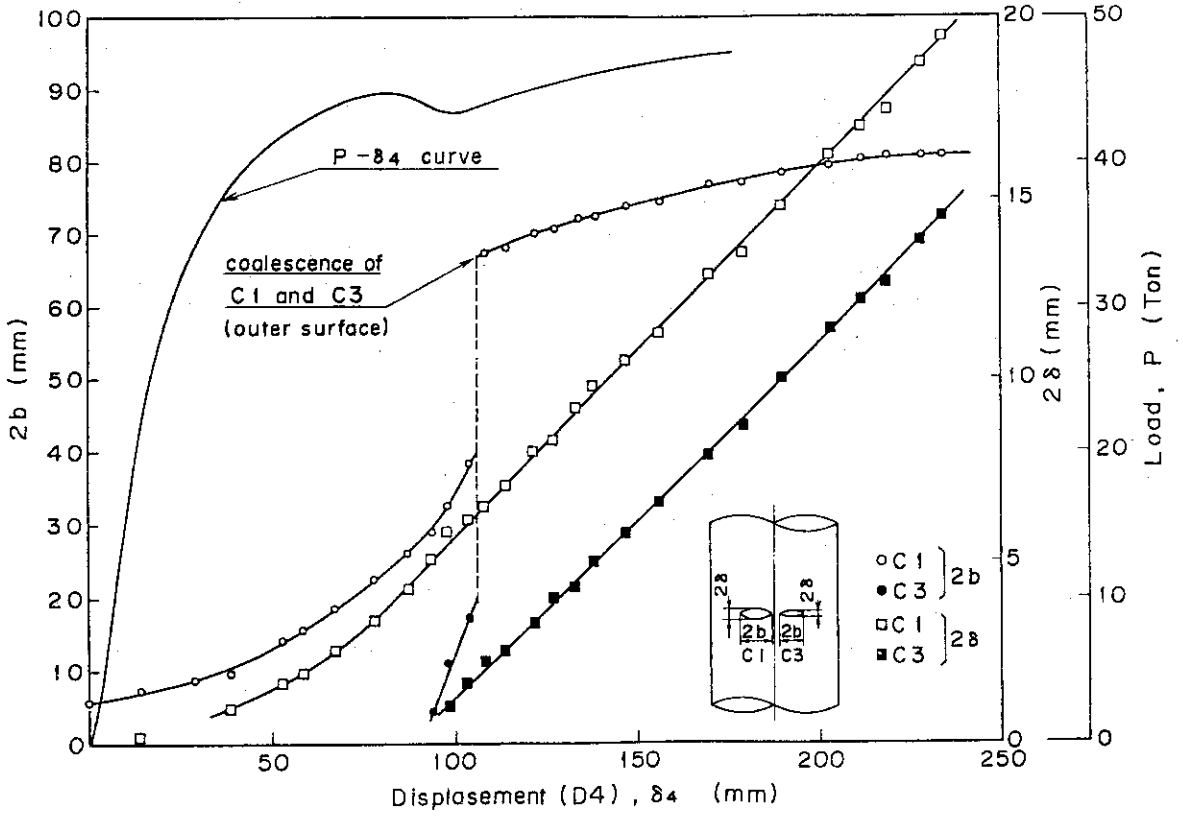

Fig. 6.12 Result of crack size and COD measurement of the outer surface in the fracture test

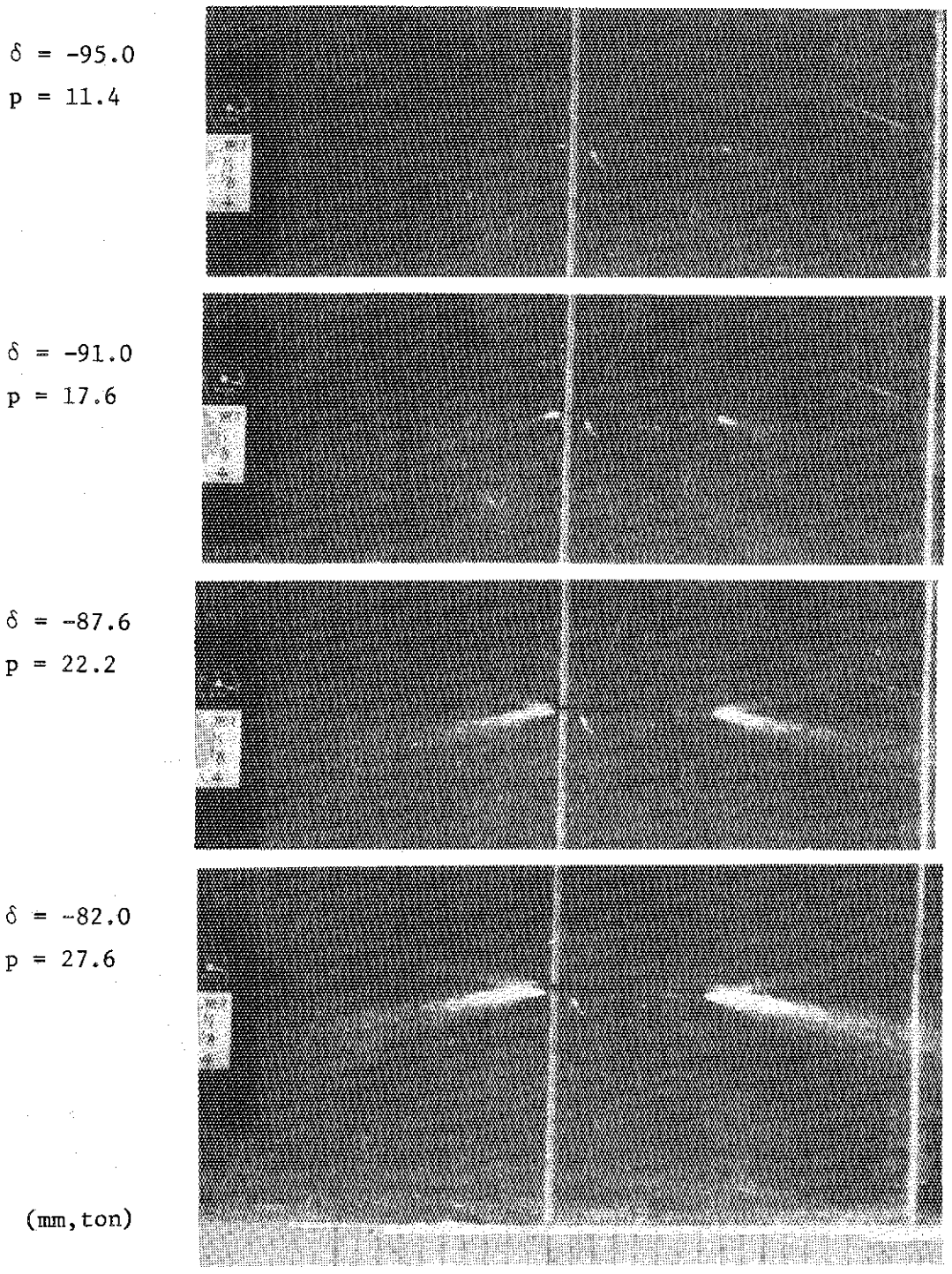

Photo. 6.1 State of the crack extension during fracture test (ST-1) (1/4)

δ = -76.0
p = 31.4

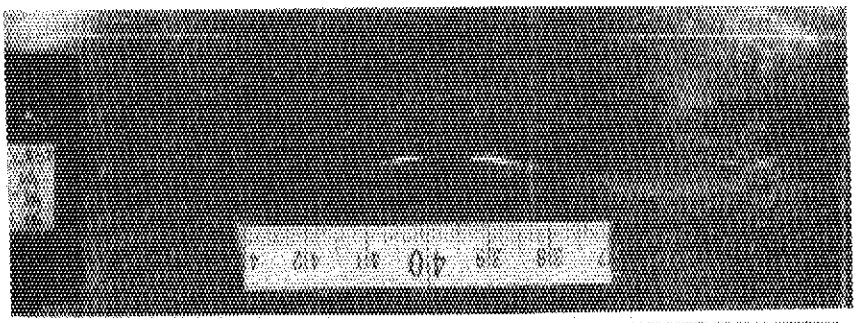

δ = -69.4
p = 34.4

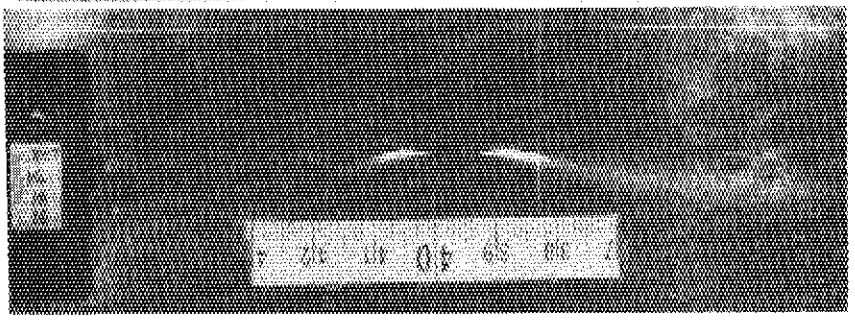

δ = -60.3
p = 37.4

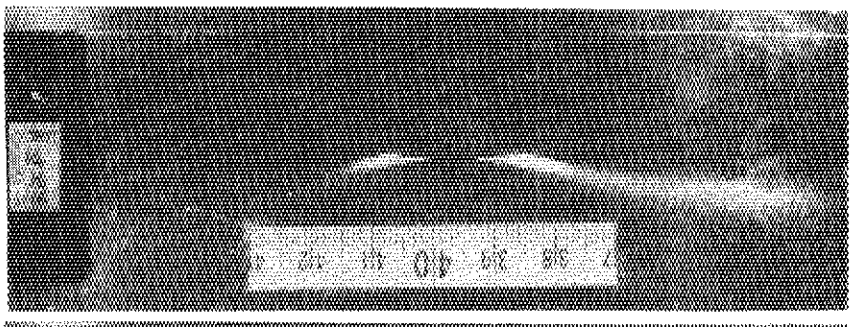

δ = -50.6
p = 39.4

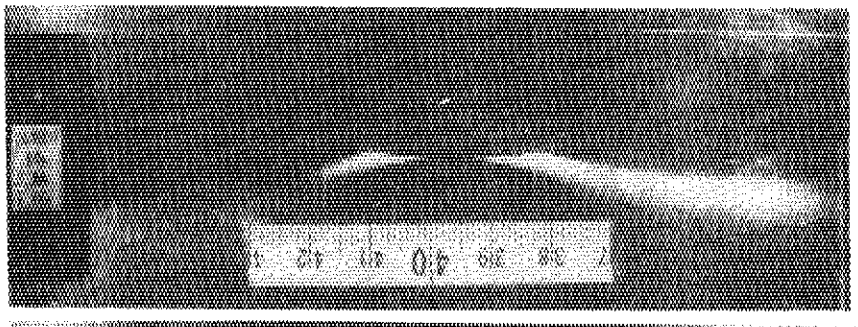

δ = -33.6
p = 41.8

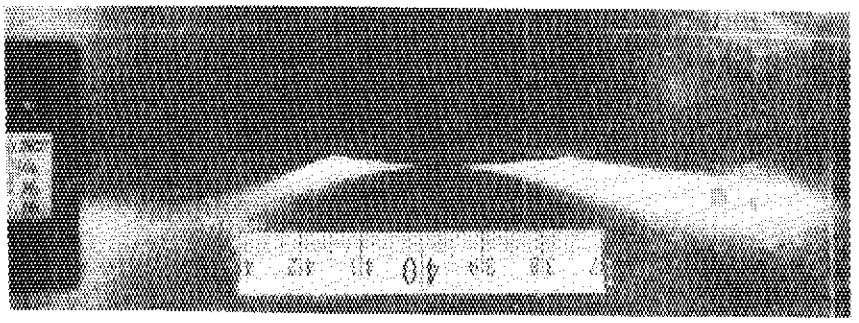

(mm, ton)

Photo. 6.1 (continued, 2/4)

δ = -19.7
p = 43.0

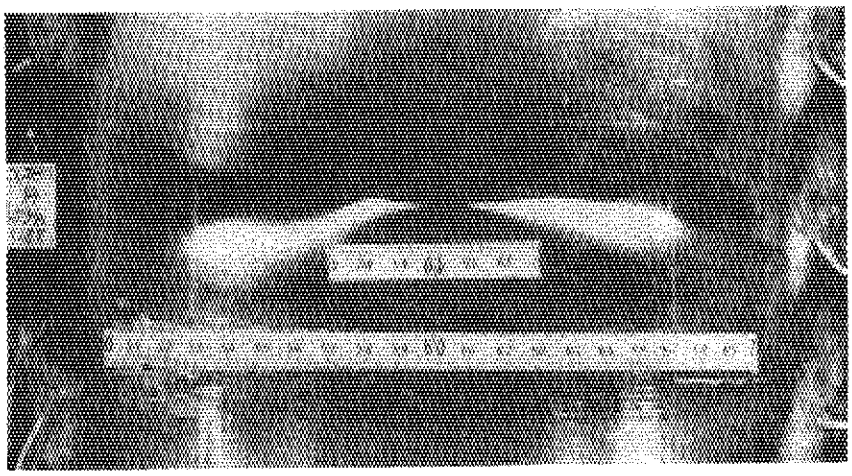

δ = 2.8
p = 44.5

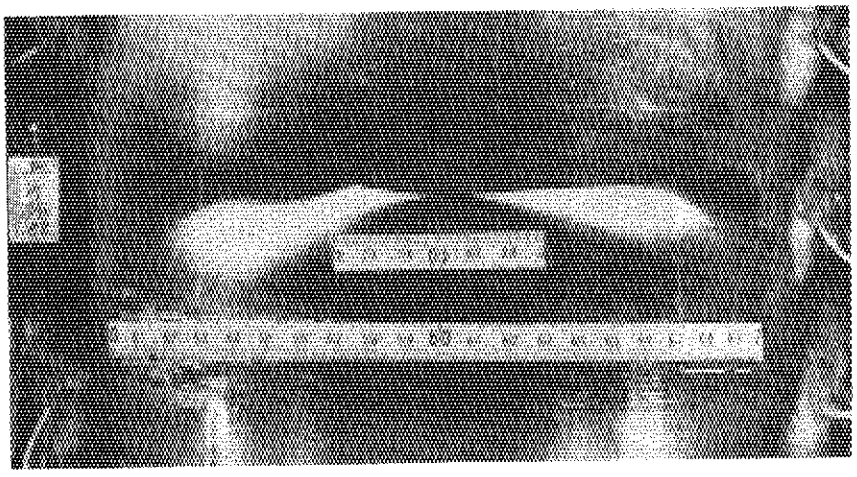

δ = 31.7
p = 45.7

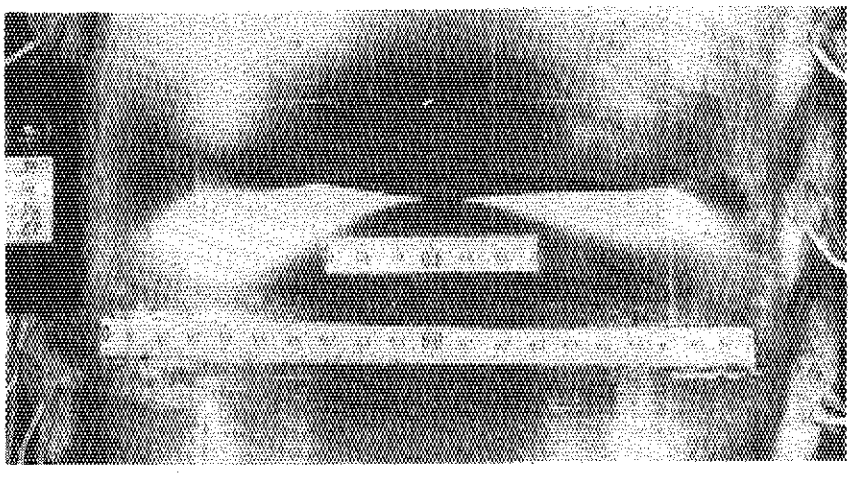

(mm, ton)

Photo. 6.1 (continued, 3/4)

δ = 53.4
p = 46.4

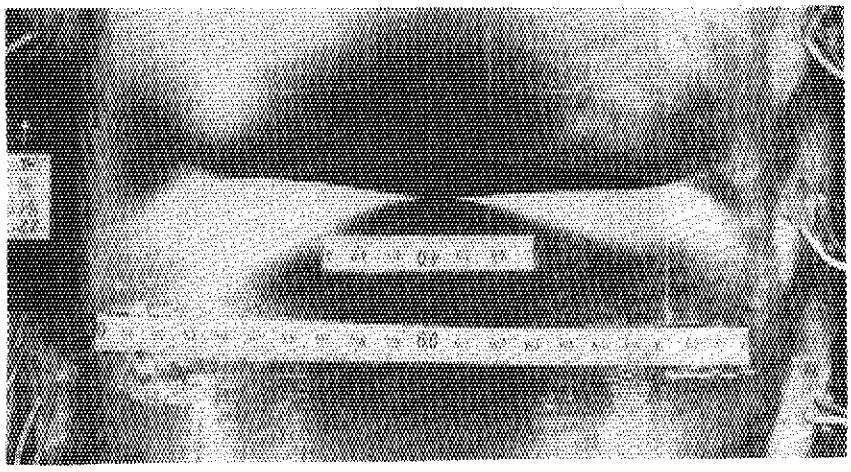

δ = 82.4
p = 47.0

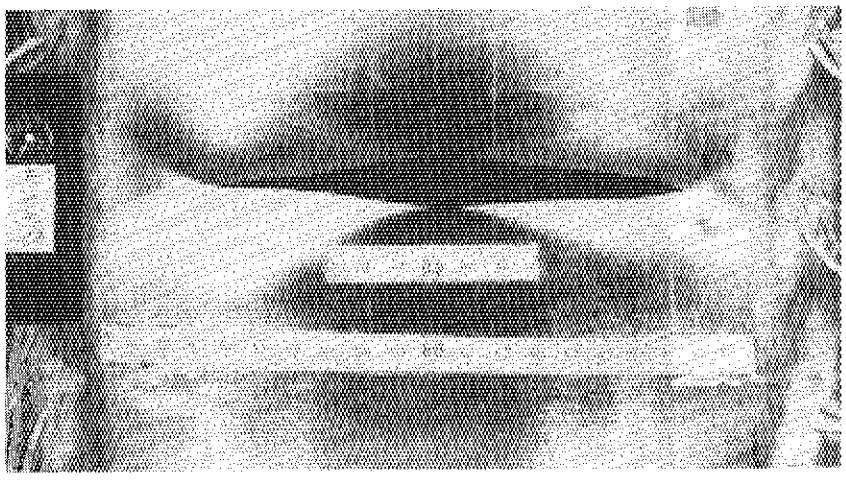

δ = 113.6
p = 49.0

(mm, ton)

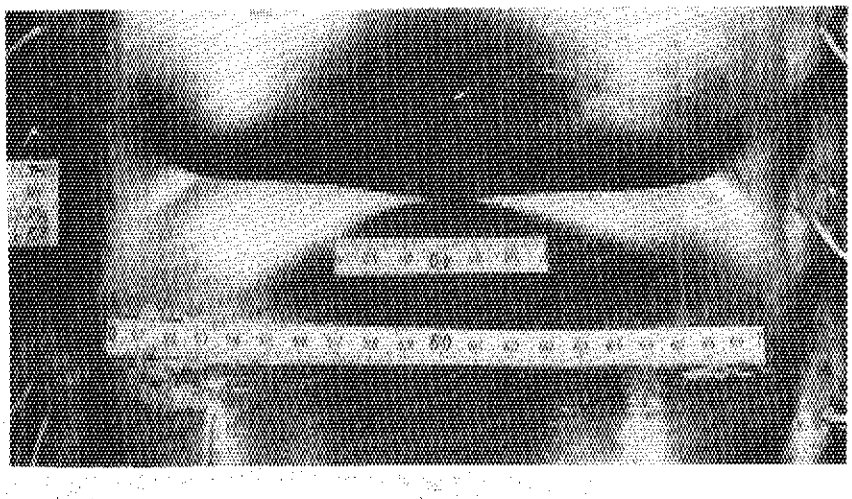

Photo. 6.1 (continued, 4/4)

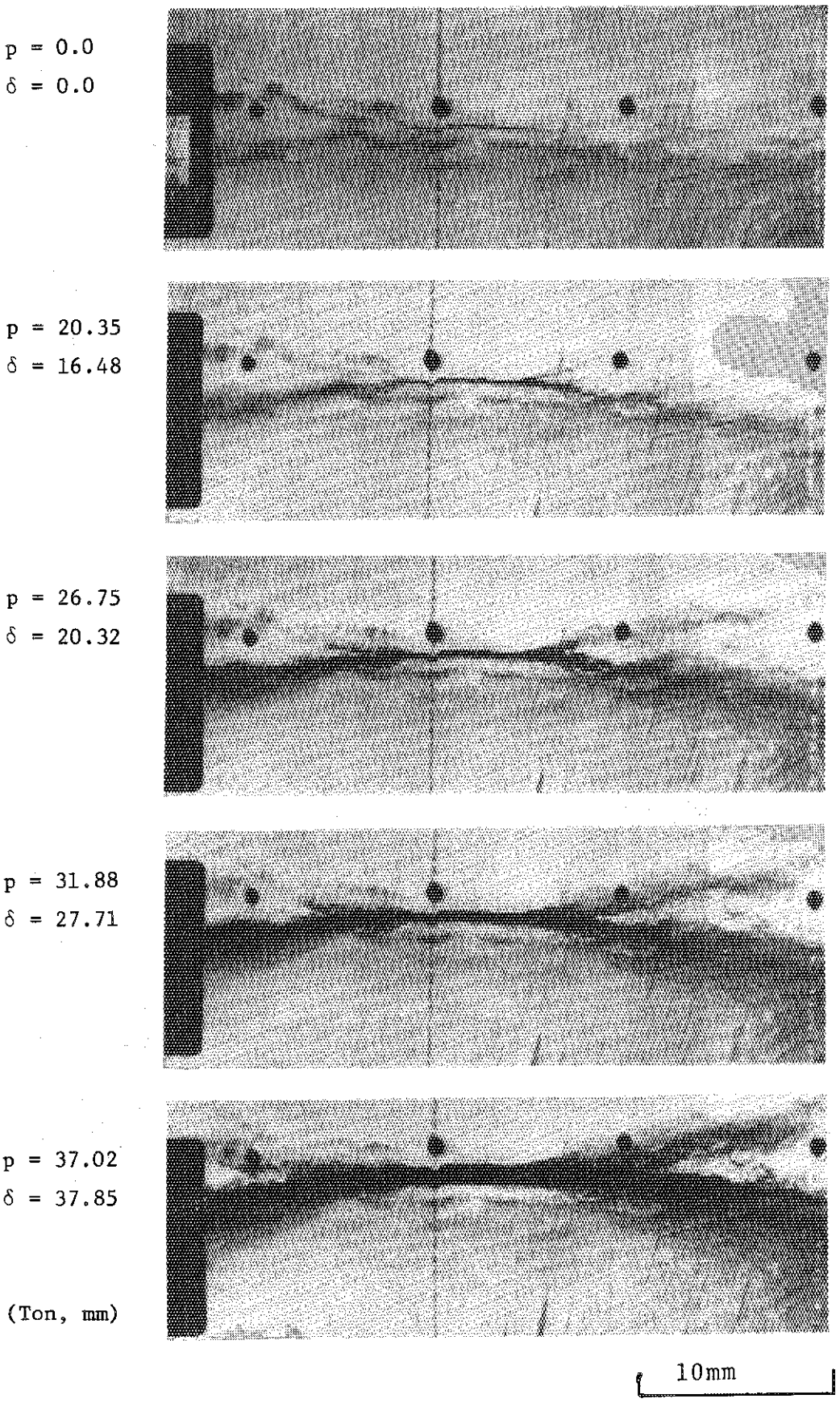

Photo. 6.2 State of the crack extension in the fracture test (ST-1) (1/4)

p = 38.67
δ = 43.45

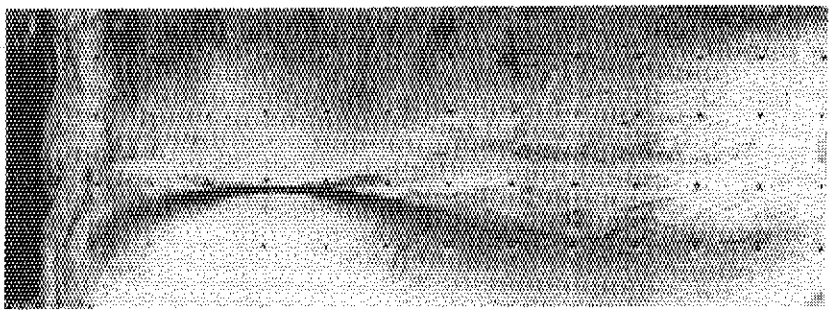

p = 40.03
δ = 47.94

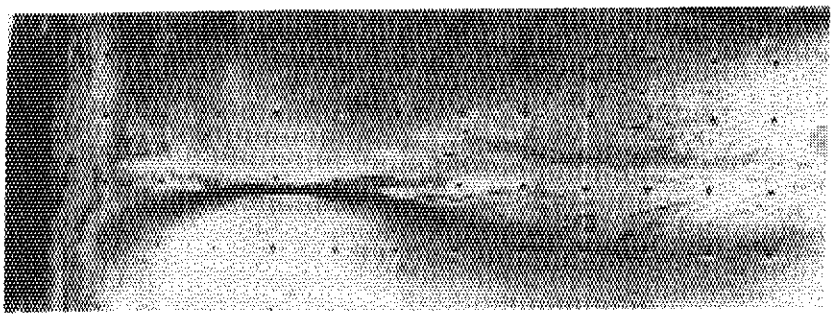

p = 42.26
δ = 59.39

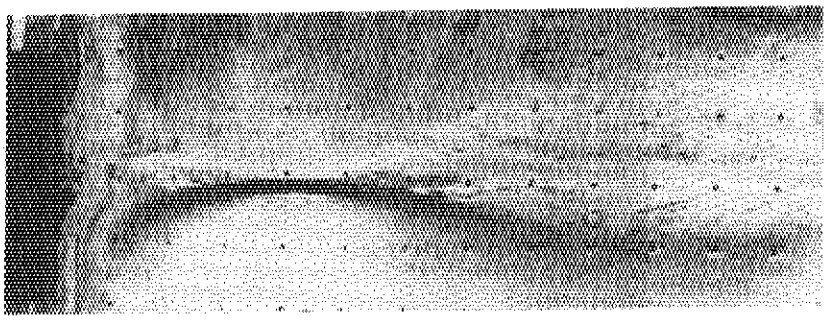

p = 43.49
δ = 68.43

p = 44.58
δ = 89.23

(Ton, mm)

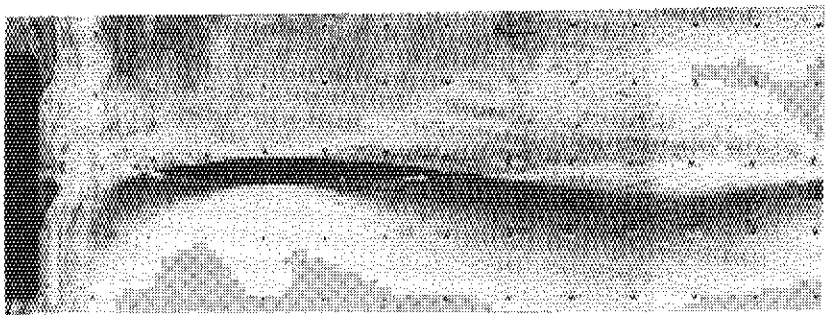

50mm

Photo. 6.2 (continued, 2/4)

p = 43.41
δ = 100.57

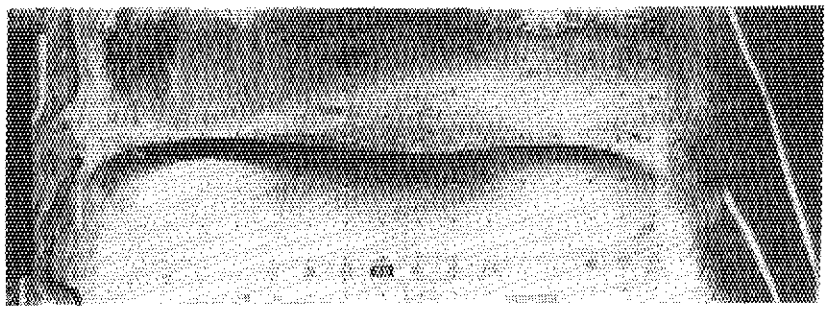

p = 43.86
δ = 113.88

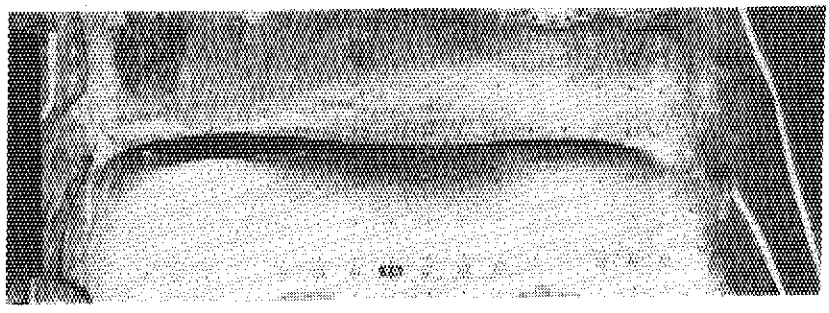

p = 44.92
δ = 129.34

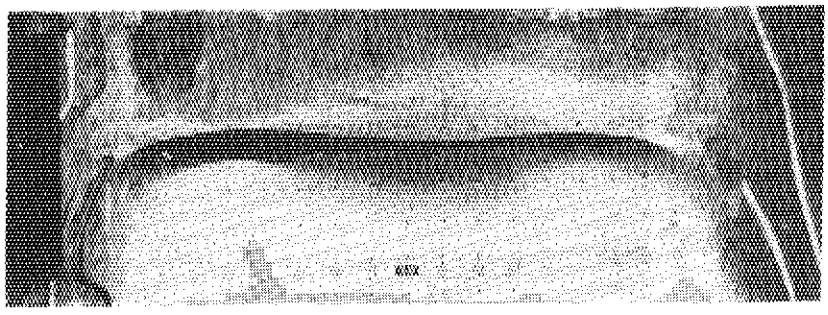

p = 45.56
δ = 140.59

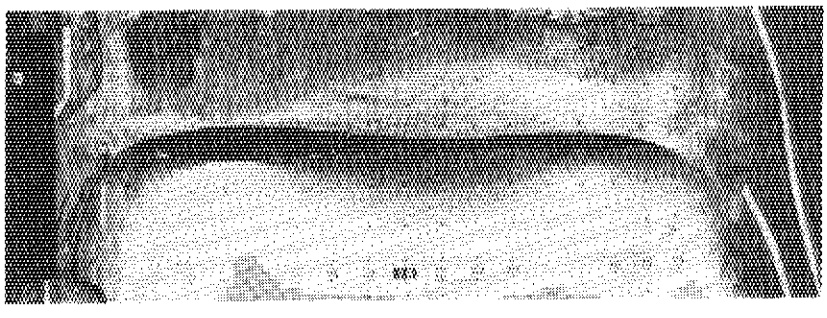

p = 46.02
δ = 149.47

(Ton, mm)

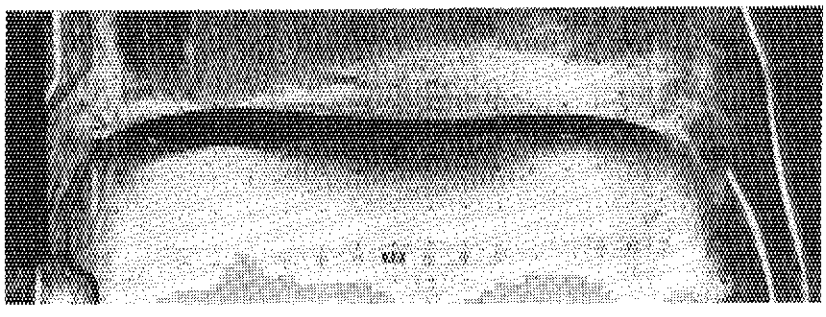

100mm

Photo. 6.2 (continued, 3/4)

p = 46.47
δ = 158.39

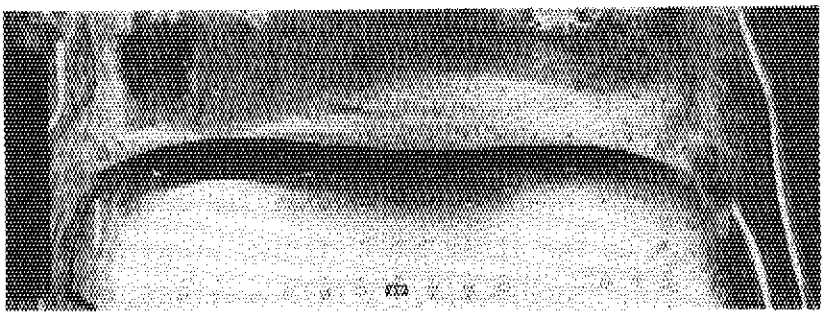

p = 47.05
δ = 170.59

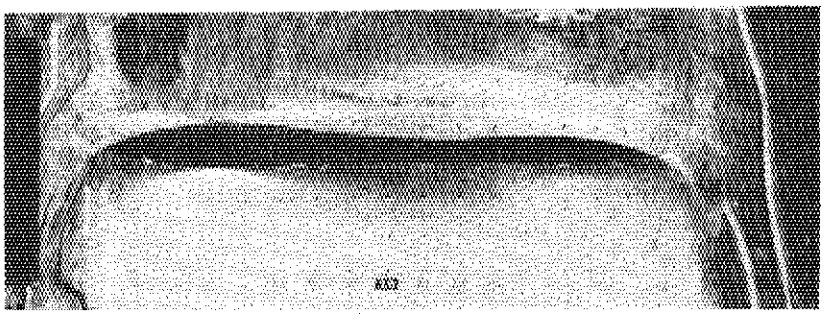

p = 48.32
δ = 201.08

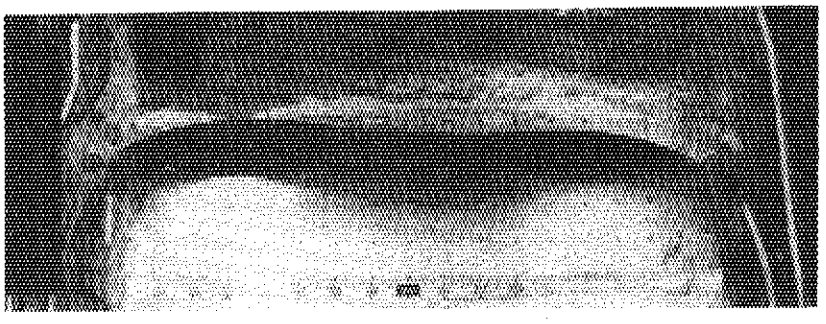

p = 48.92
δ = 219.46

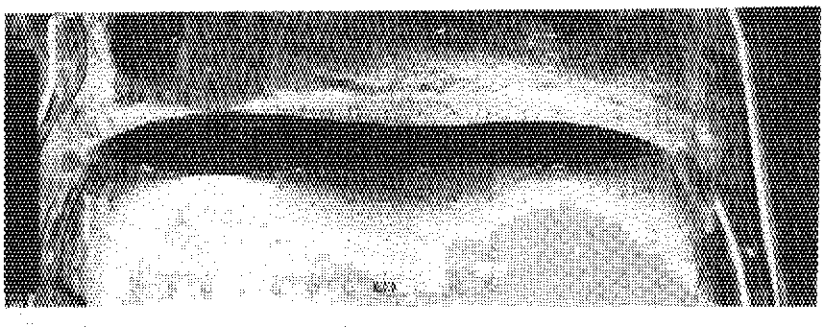

p = 48.45
δ = 235.49

(Ton, mm)

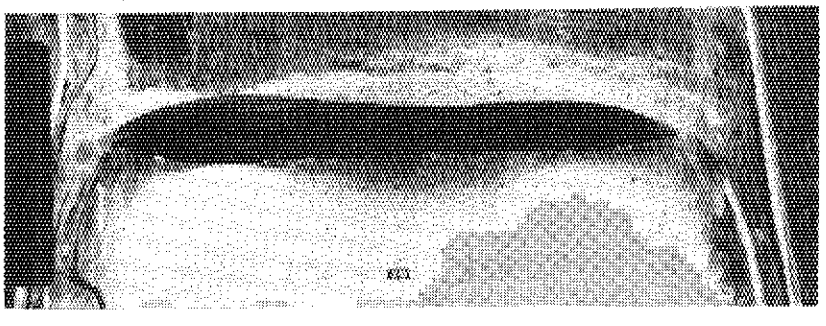

100mm

Photo. 6.2 (continued, 4/4)

7. Fractographic observation

Fractographic observations of fracture surfaces after fatigue and fracture tests were carried out by a scanning electron microscopy.

The striation was not observed at low crack growth rate as shown in Photo.7.1. On the other hand, it was observed at high crack growth rate as shown in Photo.7.1.2. A fair correspondence between striation spacing (2.8×10^{-4} mm/cycle) and optical measurement of the crack growth rate (2.3×10^{-4} mm/cycle) was obtained from Photo. 7.2.

The fractographic observation of ST-1 and ST-2 test pipes was almost the same.

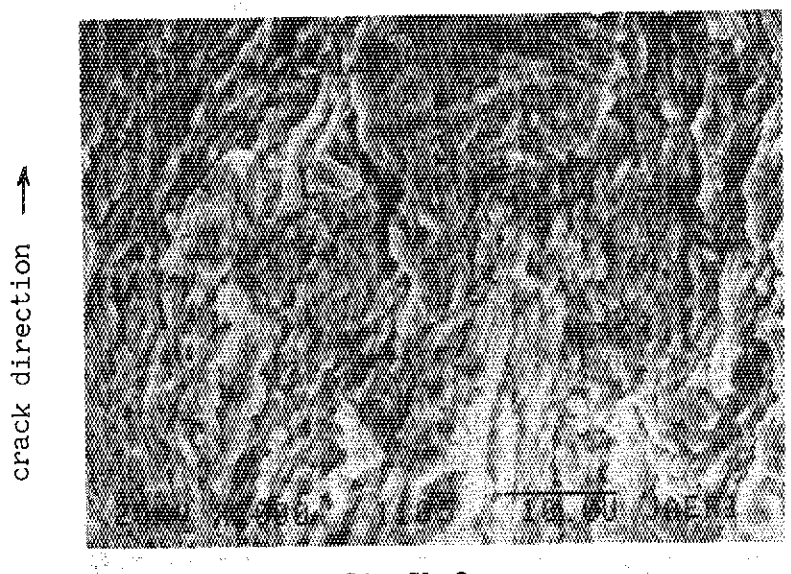

(1) crack length 13mm, C1, SL-2
magnification 2000 times

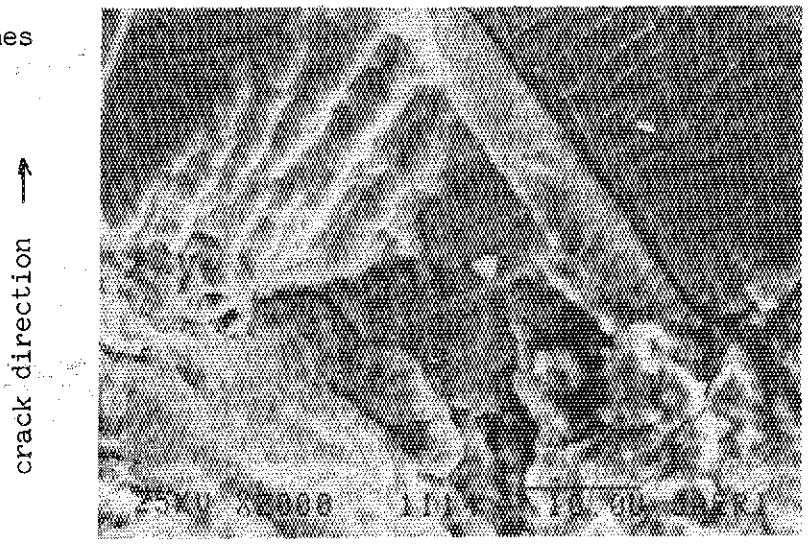

(2) crack length 29.5mm, C1, SL-2
magnification 2000 times

Photo. 7.1 Fractographs

8. Conclusions

The following conclusions are obtained from the fatigue and fracture tests of ST-1 and ST-2 test pipes.

1) The stress distribution measured by strain gages shows a good agreement with calculated results.
2) The fatigue crack passes through the wall from the C2 crack at 650,000 cycles in ST-1 test pipe. On the other hand, in ST-2 test pipe, the fatigue crack passes through the wall from C1 crack at 635,000 cycles. Both test pipes take almost the same number of cycles for passing through the wall of test pipe.
3) The thickness of the test section of ST-2 test pipe is thinner than one of ST-1 test pipe because of edge preparation in welding. Therefore the crack growth rate of ST-2 test pipe is lower than one of ST-1 test pipe.
4) The fatigue crack growth rate in the circumferential direction of ST-2 test pipe is larger than one of ST-1 test pipe, so that the crack length of the ST-2 test pipe at the end of fatigue test is longer than one of ST-1 test pipe.
5) There was a good agreement between the fatigue crack depth obtained by a beach mark and by an ultrasonic method in which an angle probe of longitudinal wave was used during the fatigue test. These experimental results show that the fatigue crack depth in the inner surface of a pipe can be quantitatively measured by an ultrosonic method and there is a capability to apply this ultrasonic method to the non-destructive inspection of nuclear power plant components.
6) The crack growth behavior during the fatigue test could be examined by the beach mark, ultrasonic method and electric potential method.
7) The experimental results of fatigue test show that the crack growth in the thickness direction is more conservative than that by the analytical method specified in the Section XI of ASME Code[2]. After three cracks coalesce by cyclic loads, there is much discrepancy between the fatigue crack growth behavior obtained by these tests and one predicted by the ASME Code. Therefore, it seems that the analytical method of the ASME Code is more severe than the phenomena practically caused.

8) After the fatigue tests were performed, the static load was imposed on both the test pipes in the fracture test. The experimental results show a tendency that the load is still increasing when the displacement is more than 200 mm, and the test pipes have enough strength and toughness for 3 S_m load specified in the Section III of ASME Code to prevent the brittle fracture, even though a large crack exists in the inner surface of the pipe.

9) The crack extension of ST-1 and ST-2 test pipes was observed from P = 30 ton, and was high over 40 ton. The crack extension proceeds with plastic deformation and is accompanied with large plastic deformation.

10) In the fracture test of ST-2 test pipe an unstable crack extension was observed locally. This experimental result shows that the local unstable fracture might be caused dependent on the effect of crack geometry or the weld condition.

11) The crack extension is low after the crack becomes a large penetrated one and the displacement is over 100 mm. The plastic deformation is mainly caused noticeably in this displacement range.

Acknowledgement

The authers would like to appreciate Dr. M. Nozawa, Head of Division of Reactor Safety, Mr. A. Morishima, Deputy Head of Division of Reactor Safety, Mr. M. Osanai, Deputy Head of Division of Reactor Safety of JAERI for their support through this work. Thanks are given to Professor Dr. Y. Ando of Tokyo University and menbers of Committee on the Assessment of Safety Research for Nuclear Reactor Structural Components for their useful discussions and suggestions.

References

1) ASME Boiler and PV. Code Sec.III (1977)

2) ASME Boiler and PV. Code Sec.XI (1977)

8) After the fatigue tests were performed, the static load was imposed on both the test pipes in the fracture test. The experimental results show a tendency that the load is still increasing when the displacement is more than 200 mm, and the test pipes have enough strength and toughness for 3 S_m load specified in the Section III of ASME Code to prevent the brittle fracture, even though a large crack exists in the inner surface of the pipe.
9) The crack extension of ST-1 and ST-2 test pipes was observed from P = 30 ton, and was high over 40 ton. The crack extension proceeds with plastic deformation and is accompanied with large plastic deformation.
10) In the fracture test of ST-2 test pipe an unstable crack extension was observed locally. This experimental result shows that the local unstable fracture might be caused dependent on the effect of crack geometry or the weld condition.
11) The crack extension is low after the crack becomes a large penetrated one and the displacement is over 100 mm. The plastic deformation is mainly caused noticeably in this displacement range.

Acknowledgement

The authers would like to appreciate Dr. M. Nozawa, Head of Division of Reactor Safety, Mr. A. Morishima, Deputy Head of Division of Reactor Safety, Mr. M. Osanai, Deputy Head of Division of Reactor Safety of JAERI for their support through this work. Thanks are given to Professor Dr. Y. Ando of Tokyo University and menbers of Committee on the Assessment of Safety Research for Nuclear Reactor Structural Components for their useful discussions and suggestions.

References

1) ASME Boiler and PV. Code Sec.III (1977)
2) ASME Boiler and PV. Code Sec.XI (1977)